耐震性評価のための地盤調査・土質試験の運用事例ワークショップ
土木学会，2021.11.16

降雨や地震による地盤災害と地盤調査

渦岡良介

京都大学防災研究所

6th International Conference on Engineering Geophysics
Al Ain, UAE, 25 – 28 October 2021

Role of geophysical survey in geotechnical seismic analysis

地盤の動的解析における物理探査の役割

UZUOKA Ryosuke
Disaster Prevention Research Institute
Kyoto University

Outline and Acknowledgements

- Slope behavior during rainfall and earthquake

  - Matsumaru, T. and Uzuoka, R.: Three-Phase Seepage-Deformation Coupled Analysis about Unsaturated Embankment Damaged by Earthquake, International Journal of Geomechanics, 16(5), 2016. https://doi.org/10.1061/(ASCE)GM.1943-5622.0000699
  - Xu, J., Ueda, K., & Uzuoka, R. (2021). Evaluation of failure of slopes with shaking-induced cracks in response to rainfall. Landslides 2021, 1–18. https://doi.org/10.1007/S10346-021-01734-1

- Recent geophysical survey

  - Inazaki, T., Hayashi, K., Watanabe, F., Matsuo, K., Tokumaru, T., and Imamura, S., 2008. Ground truth verification of an integrated geophysical investigation for the assessment of an earthen levee. Proceedings of the 21th Annual Symposium on the Application of Geophysics to Engineering and Environmental Problems (SAGEEP2008).
  - Takahashi, T., 2018. Soil permeability profiling using geophysical data. Annual Conference of Japanese Society of Irrigation, Drainage and Rural Engineering, 2018. (in Japanese)
  - Suzaki, A., Minato, S., Ghose, R., Konishi, C., & Sakai, N., 2017. Modelling time-lapse shear-wave velocity changes in an unsaturated soil embankment due to water infiltration and drainage. First Break, 35(8), 81-90.
  - Thomas Planès, Justin B. Rittgers, Michael A. Mooney, Wim Kanning, Deyan Draganov, 2017. Monitoring the tidal response of a sea levee with ambient seismic noise. Journal of Applied Geophysics, 138, 255-263.

地盤の動的解析における物理探査（地盤調査）

- 良質な不かく乱試料を用いた室内試験がない場合、原位置試験から力学的材料パラメータを経験的に推定する場合がある。物理探査で力学的材料パラメータを合理的に推定できると有用。
- 地震前の斜面や盛土の初期条件（地下水位、飽和度分布）がその後の地震時挙動に影響するので正確に把握する必要がある。物理探査が時々刻々変化する初期条件をを推定できると有用。
- 地震後の斜面や盛土の変状がその後の降雨浸透挙動に影響する。地震後の斜面や盛土内の状態を物理探査で知ることができると有用。

Overview of numerical method

Soil-water-air coupled analysis

- Porous media theory at finite strain (de Boer 2000, Schrefler 2002)
  - Soil skeleton, pore water and pore air
  - Static, quasi-static and dynamic problem
- Balance equations
  - Mass and momentum balances of soil skeleton
  - Mass and momentum balances of pore water
  - Mass and momentum balances of pore air
- Constitutive models
  - Bishop’s effective stress (skeleton stress)
  - Darcy flow: interaction between soil skeleton and fluid
  - Compressibility of pore water
  - Compressibility of pore air
  - Water retention curve (SWCC, WRC)
  - Constitutive model for soil skeleton
    - Cyclic elasto-plastic model, etc.
- Numerical method
  - Mixed finite element method
  - Newmark time integration

Numerical analysis flow

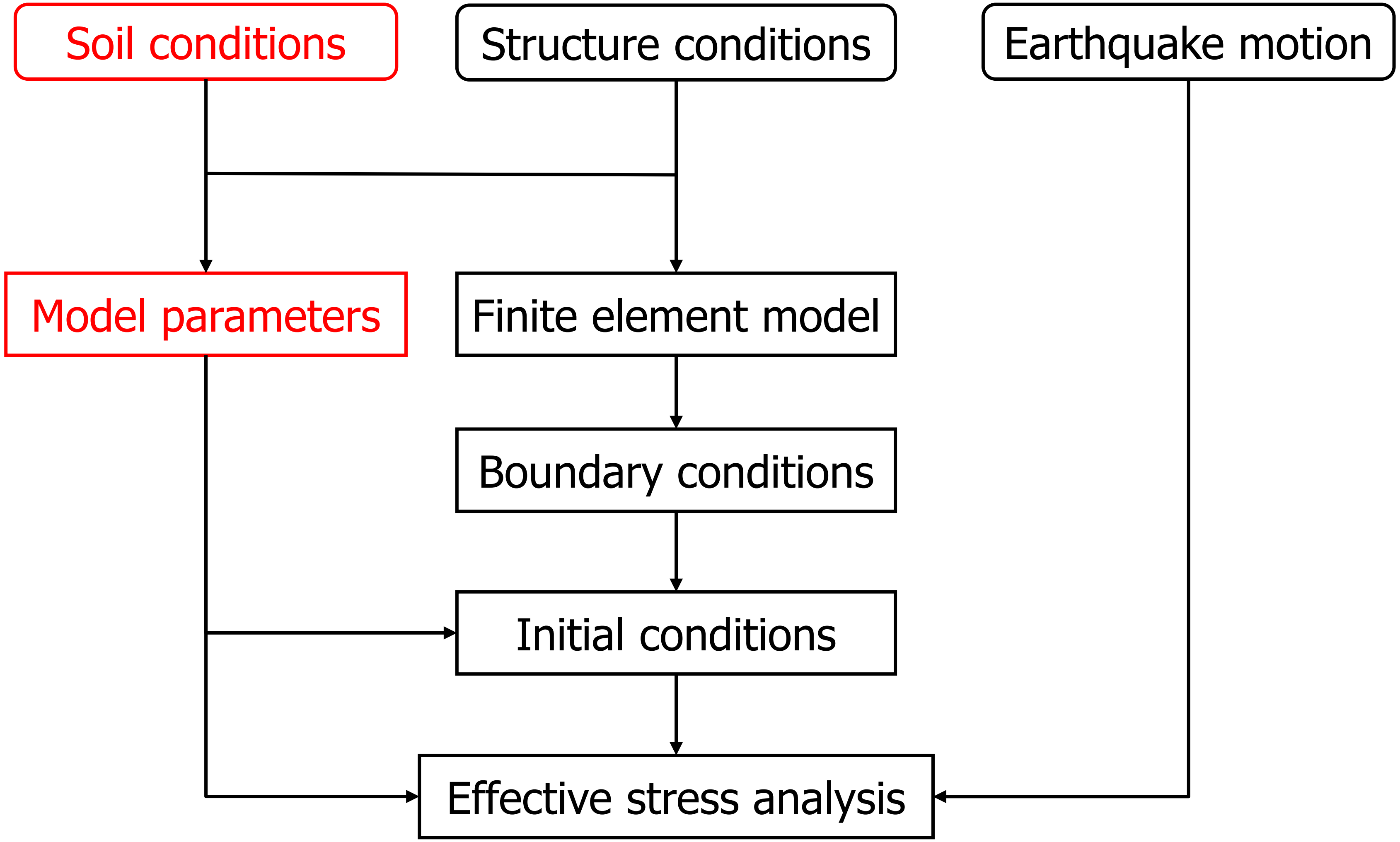

Model parameters

- In-situ tests
  - SPT (N-value, Soil profile, ground water)
  - PS logging (S and P wave velocity)
- Laboratory tests with disturbed samples
  - Particle size distribution test
  - Permeability test
- Laboratory tests with undisturbed samples
  - Density test
  - Consolidation test (compression and swelling indexes)
  - Shear test (friction and dilatancy angle)
  - Undrained cyclic shear test (strain-dependent shear stiffness and damping, liquefaction strength)
- When you do not have high quality undisturbed samples,
  - Give up the analysis
  - Use empirical relationship with in-situ test output

Simulation of laboratory tests

- Undrained/drained monotonic/cyclic shear tests
- Stress – strain relationship, stress path
- Strain-dependent stiffness/damping, liquefaction strength curve

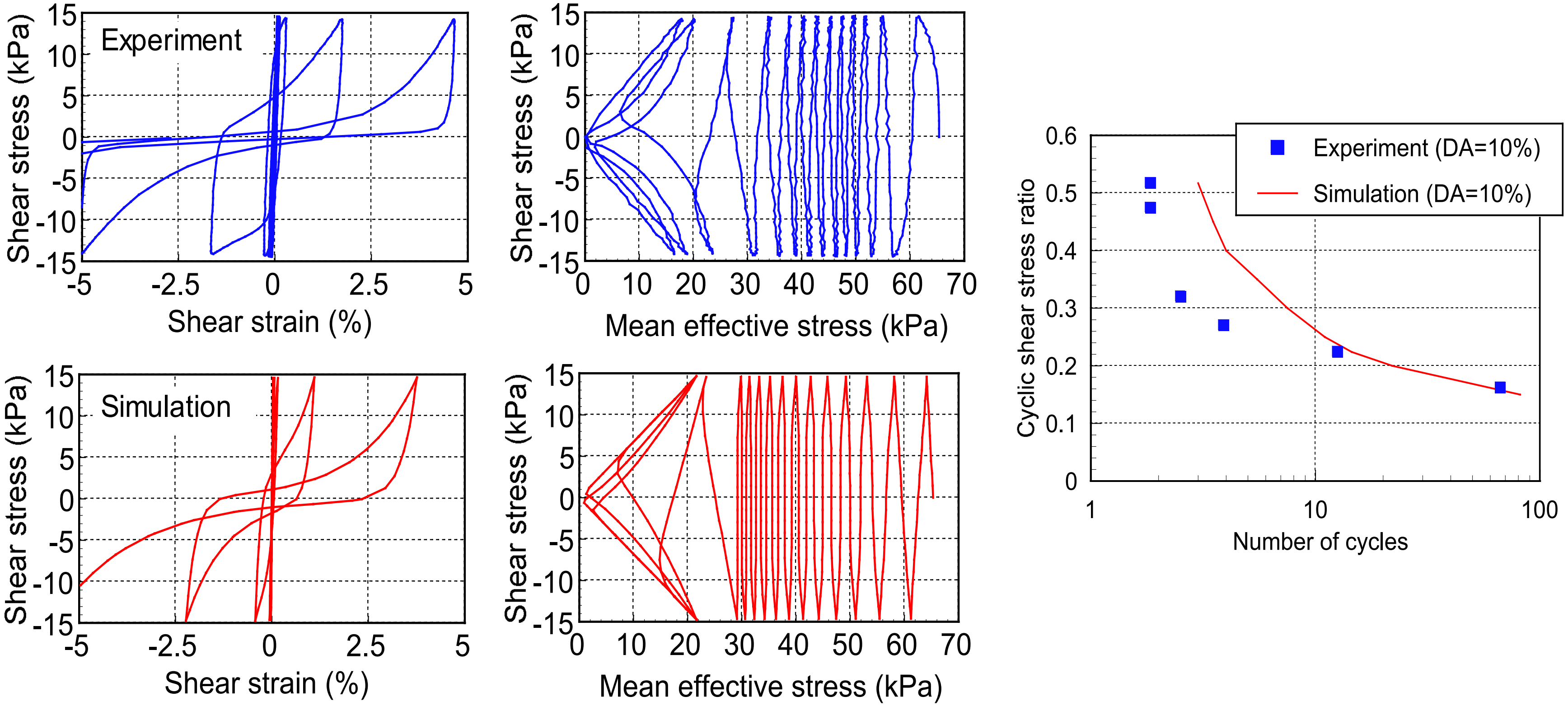

(a) Shear stress - shear strain relations (b) Effective stress paths

Liquefaction resistance by in-situ sounding

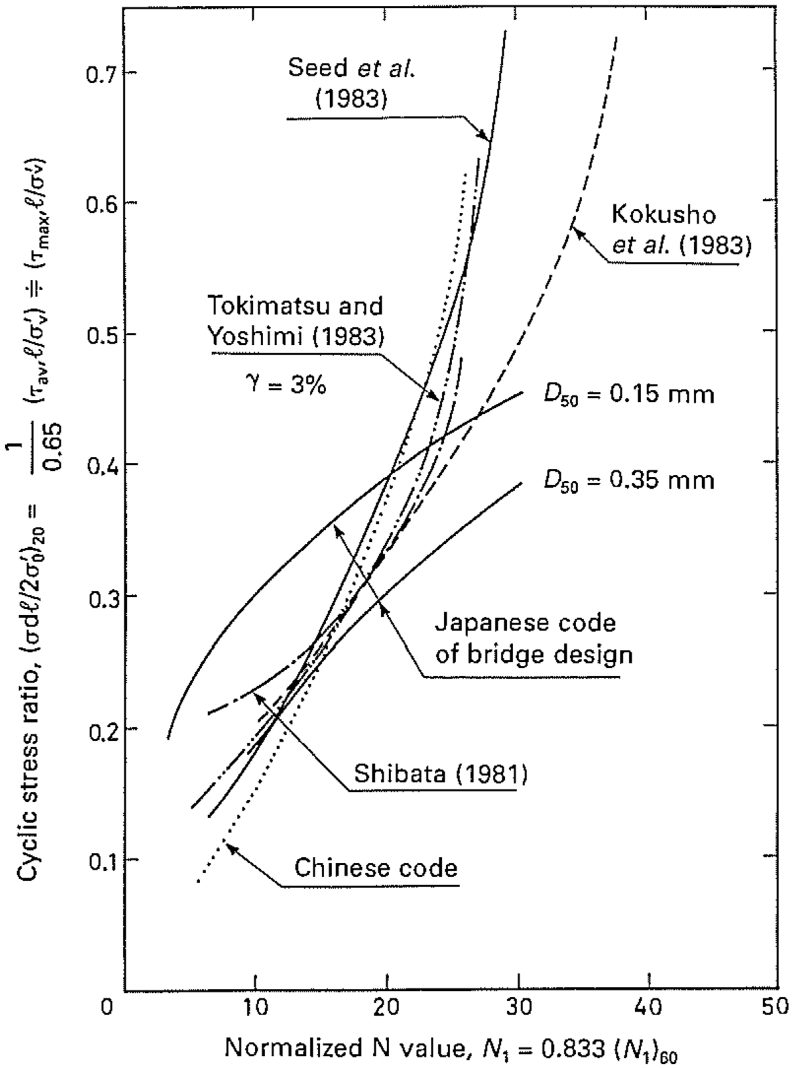

Fig. 12.2 Summary chart for evaluation of the cyclic strength of sands based on the normalized SPT *N* value.

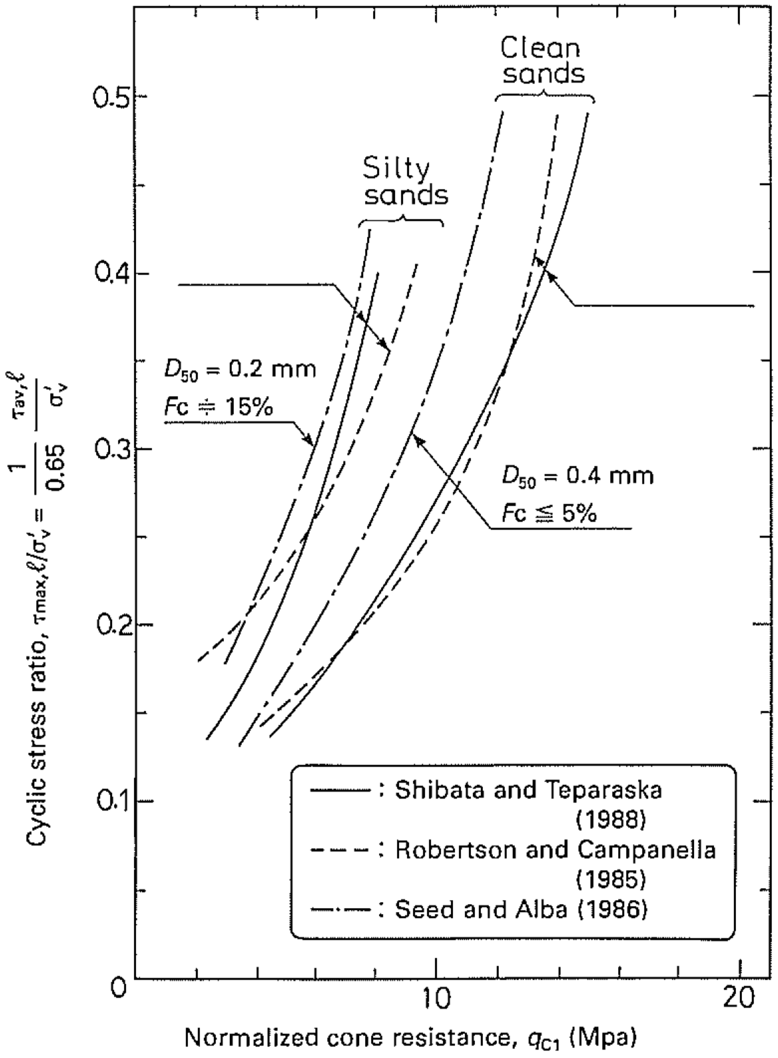

Fig. 12.3 Summary chart for evaluation of the cyclic strength of sands based on the normalized CPT q_c value.

Soil Behaviour in Earthquake Geotechnics (Ishihara, 1996)

Shear wave velocity by in-situ sounding

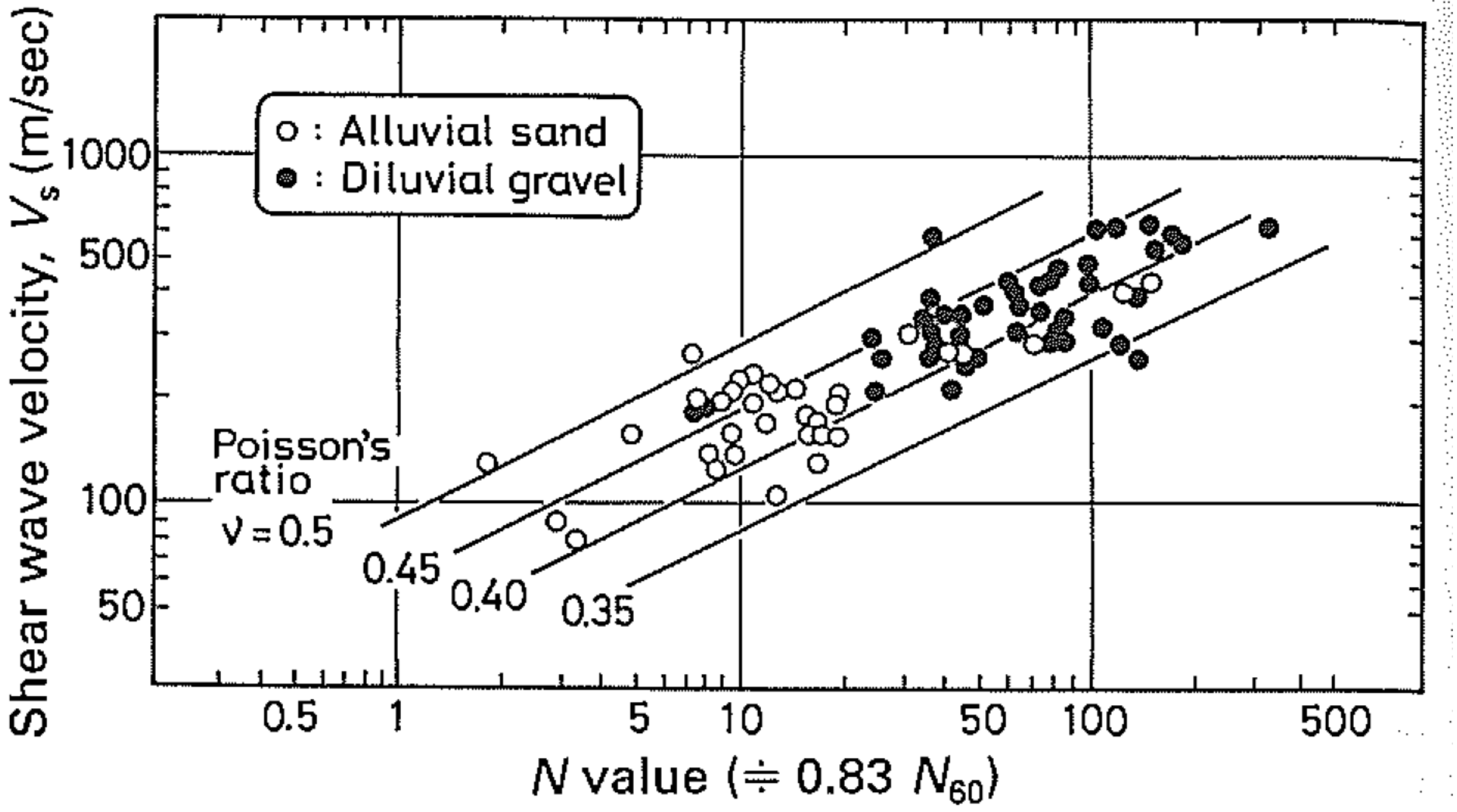

Fig. 6.32 Relation between shear wave velocity and *N* value of SPT (Imai and Yoshimura, 1972).

Soil Behaviour in Earthquake Geotechnics (Ishihara, 1996)

Soil dynamics

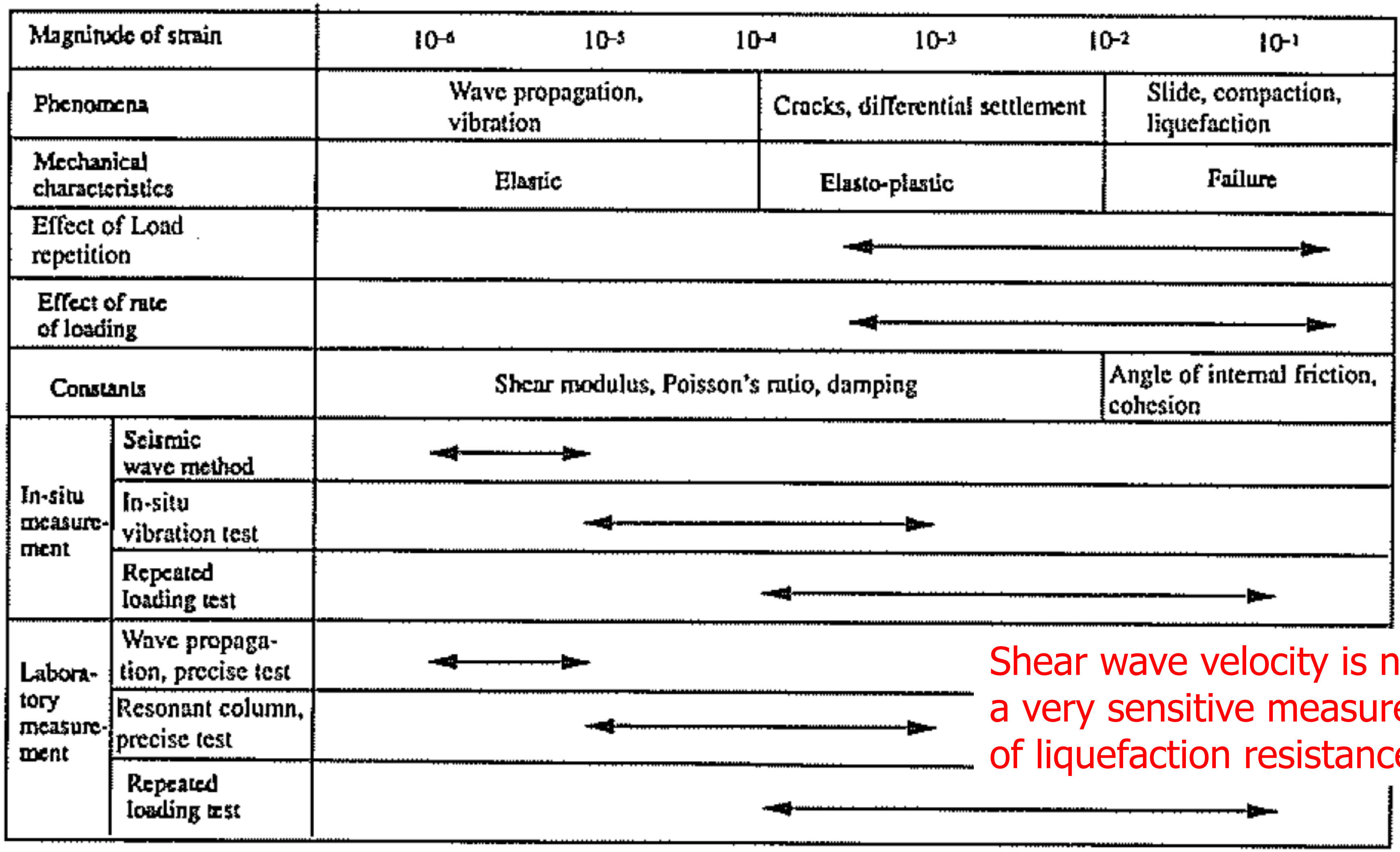

Shear wave velocity is not a very sensitive measure of liquefaction resistance.

Fig. 1.2 Variation of soil properties with strain.

Soil Behaviour in Earthquake Geotechnics (Ishihara, 1996)

地盤の動的解析における物理探査（地盤調査）

- 良質な不かく乱試料を用いた室内試験がない場合、原位置試験から力学的材料パラメータを経験的に推定する場合がある。物理探査で力学的材料パラメータを合理的に推定できると有用。
- 地震前の斜面や盛土の初期条件（地下水位、飽和度分布）がその後の地震時挙動に影響するので正確に把握する必要がある。物理探査が時々刻々変化する初期条件をを推定できると有用。
- 地震後の斜面や盛土の変状がその後の降雨浸透挙動に影響する。地震後の斜面や盛土内の状態を物理探査で知ることができると有用。

Matsumaru, T. and Uzuoka, R.: Three-Phase Seepage-Deformation Coupled Analysis about Unsaturated Embankment Damaged by Earthquake, International Journal of Geomechanics, 16(5), 2016. https://doi.org/10.1061/(ASCE)GM.1943-5622.0000699

Background

The 2004 Niigata-ken Chuetsu earthquake (23rd Oct.) caused wide-spread area damages of embankments.

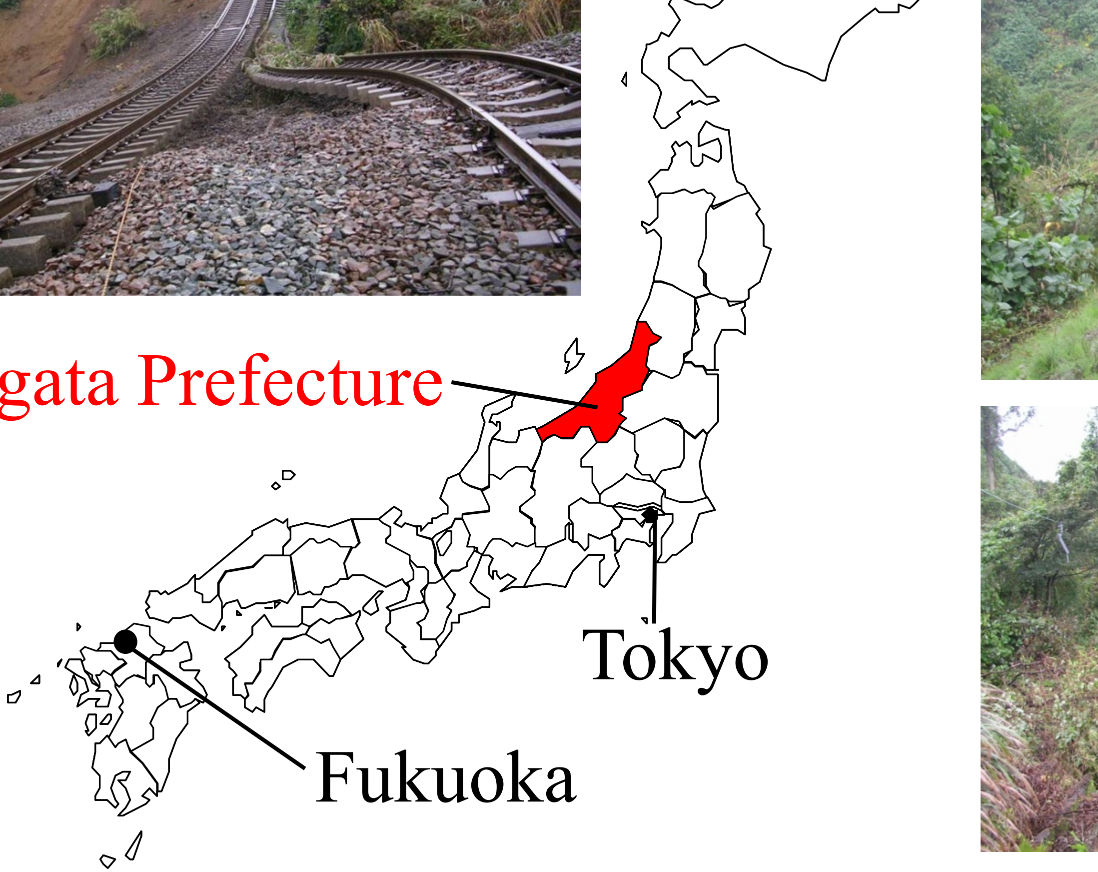

Purpose

- Nigata Prefecture was affected by the rainfall before this earthquake.

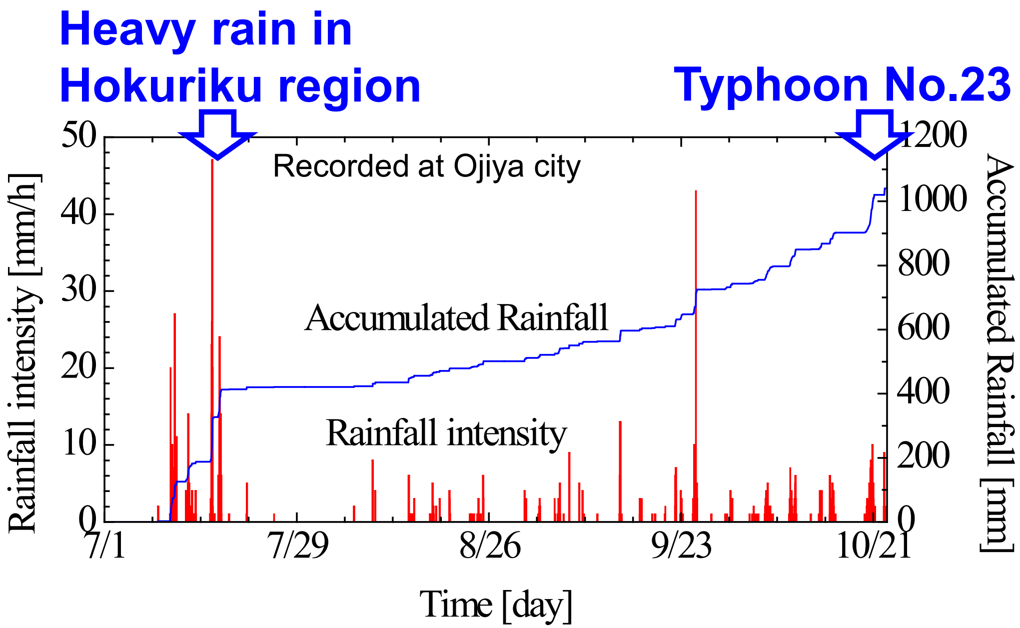

Main reason of the damages?

However, there are a small number of researches about seismic behavior considering rainfall.

Three-phase seepage-deformation coupled FE analysis focused on this damage was performed.

Basic function

Overall density of mixture

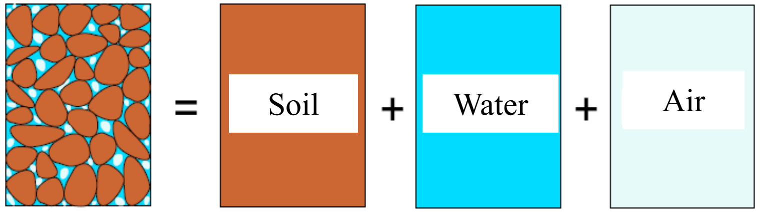

$$\rho = \rho^{s} + \rho^{w} + \rho^{a}$$
$$= (1-n)\rho^{sR} + n\left\{ s^{w}\rho^{wR} + (1-s^{w})\rho^{aR} \right\}$$

Skeleton stress (e.g. Gallipol et al. 2003)

$$\boldsymbol{\sigma}' = \boldsymbol{\sigma} - p^{a}\mathbf{I} + s^{w}\left(p^{a} - p^{w}\right)\mathbf{I}$$

Gallipoli, D., Gens, A., Sharma, R. and Vaunat, J.: An elasto-plastic model for unsaturated soil incorporating the effects of suction and degree of saturation on mechanical behavior, Geotechnique, Vol.53, No.1, pp.123-135, 2003.

Soil Water Characteristic Curve(Sugii et al. 2002)

$$s^{w} = \left(s_{s}^{w} - s_{r}^{w}\right)s_{e}^{w} + s_{r}^{w} \qquad s_{e}^{w} = \left\{1 + \exp\left(a_{\lg} p^{c} + b_{\lg}\right)\right\}^{-c_{\lg}}$$

Sugii, T., Yamada, K. and Kondou, T. 2002. Rela-tionship between soil-water characteristic curve and void ratio, Proceedings of emational Conference, 1: 209-214.

Permeability coefficient of water and air

$$k^{ws} = k_{s}^{w}\left(s_{e}^{w}\right)^{\xi_{k}} \qquad k^{as} = k_{s}^{a}\left(1 - s_{e}^{w}\right)^{\eta_{k}}$$

Constitutive model for unsaturated soil (1)

Yield function

$$f = \sqrt{\frac{3}{2}}\|\boldsymbol{\eta} - \boldsymbol{\alpha}\| - k = 0$$

Nonlinear evolution rule

(Armstrong and Frederick, 1966)

$$\dot{\boldsymbol{\alpha}} = a\left(\frac{2}{3}b\dot{\mathbf{e}}^{p} - \boldsymbol{\alpha}\dot{\varepsilon}_{d}^{p}\right)$$

Armstrong. P. J. and Frederick. C.O.: A mathematical representation of the multiaxial Bauschinger effect, Technical report C.E.G.B.Report RD/B/N731, Berkeley Nuclear Laboratories, 1966.

In order to describe the large strain

a is reduced according to the value of the equivalent plastic strain $\varepsilon_d^{p(n)}$

$$a = a_0 - \frac{(a_0 - a_1)}{1 + (a_0 - a_1)\exp\left(-C_f \varepsilon_d^{p(n)}\right)}$$

Constitutive model for unsaturated soil (2)

Non-associated flow rule

$$\dot{\mathbf{e}}^p = \dot{\gamma}\frac{\partial g}{\partial \mathbf{s}} \qquad \dot{\varepsilon}_v^p = D\dot{\gamma}\frac{\partial g}{\partial p}$$

Plastic potential function

$$g = \sqrt{\frac{3}{2}}\left\|\boldsymbol{\eta} - \boldsymbol{\alpha}\right\| + M_m \ln\left(\frac{p}{p_a}\right)$$

In order to describe cyclic loading of unsaturated soil

The volumetric strain ε_v^p is changed depending on the suction p^c of unsaturated soil

$$D = D_1 + (D_0 - D_1)\exp\left(-p^c / p_{ref}^c\right)$$

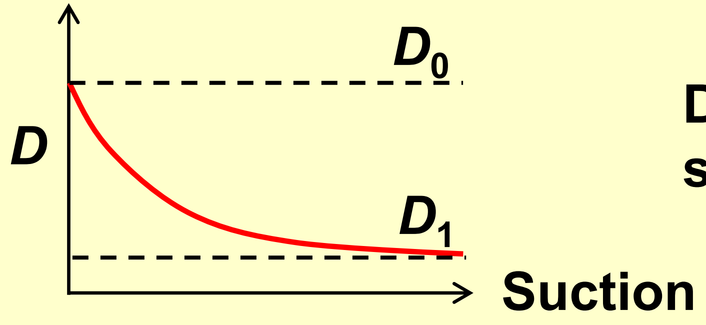

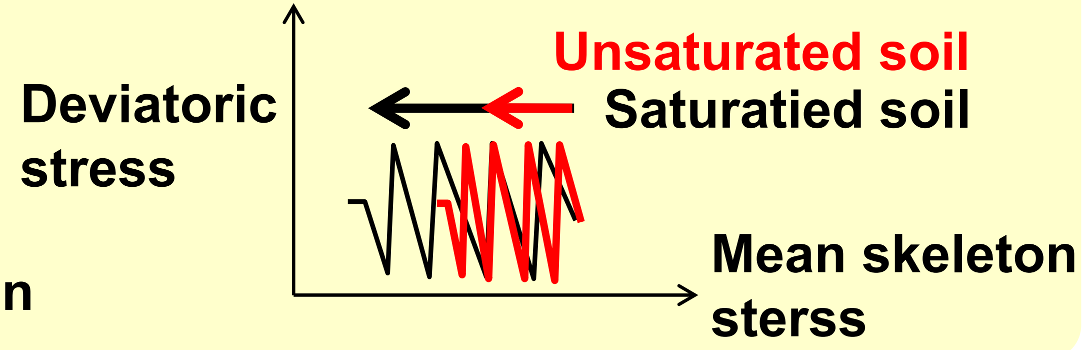

Governing equations (Uzuoka and Borja, 2012)

The momentum balance equation of the overall three phase material

$$\rho \mathbf{a}^s = div\left[\boldsymbol{\sigma}' - \left\{s^w p^w + (1 - s^w) p^a\right\}\mathbf{I}\right] + \rho \mathbf{b}$$

The mass and momentum balance equations of the pore water and air

$$\left(\frac{n s^w \rho^{wR}}{K^w} - n\rho^{wR} c\right)\frac{D^s p^w}{Dt} + n\rho^{wR} c \frac{D^s p^a}{Dt} + s^w \rho^{wR} \mathrm{div}\mathbf{v}^s + \mathrm{div}\left\{\frac{k^{ws}}{g}\left(-\mathrm{grad}p^w + \rho^{wR}\mathbf{b}^w - \rho^{wR}\mathbf{a}^s\right)\right\} = 0$$

$$\left(\frac{n\left(1 - s^w\right)M^a}{\Theta R} - n\rho^{aR} c\right)\frac{D^s p^a}{Dt} + n\rho^{aR} c \frac{D^s p^w}{Dt} + \left(1 - s^w\right)\rho^{aR} \mathrm{div}\mathbf{v}^s + \mathrm{div}\left\{\frac{k^{as}}{g}\left(-\mathrm{grad}p^a + \rho^{aR}\mathbf{b}^a - \rho^{aR}\mathbf{a}^s\right)\right\} = 0$$

Uzuoka, R. and Borja, R.I.: Dynamics of unsaturated poro-elastic solids at finite strain, *International Journal for Numerical and Analytical Methods in Geomechanics*, Vol.36, pp.1535-1573, 2012.

Outline of damaged embankment

Embankment in vicinity Joetsu Line 220k300m

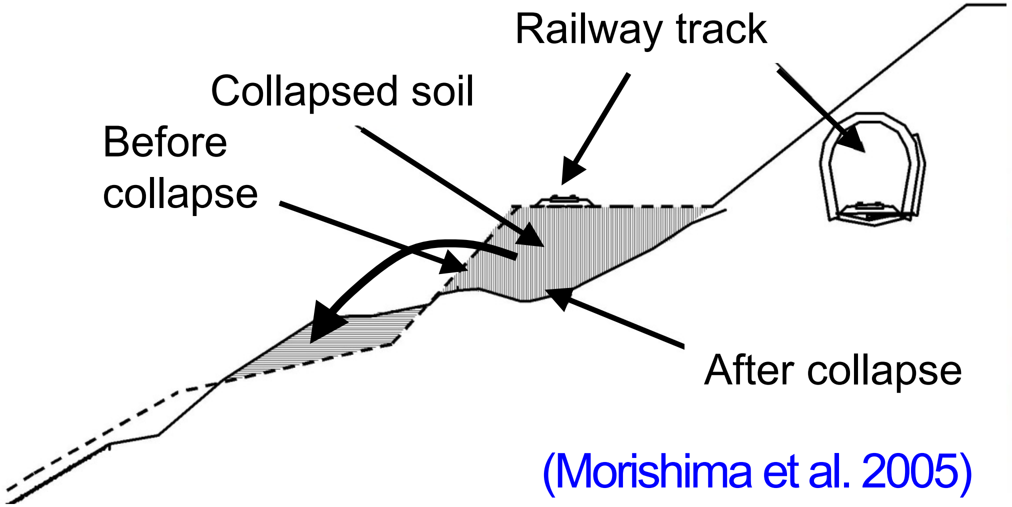

- Embankment was constructed in a valley of the Shinano River.
- The volume of collapsed soil was about 9,000 m^3.
- The damaged area had a height of 7 m.

Embankment material

G_s	D_{50}	U_c	F_c	ρ_d
2.629	0.134mm	11.65	23.3%	1.29g/cm^3

Cyclic triaxial test of embankment material

Embankment material

G_s	D_{50}	U_c	F_c	ρ_d
2.629	0.134mm	11.65	23.3%	1.29g/cm³

Procedure

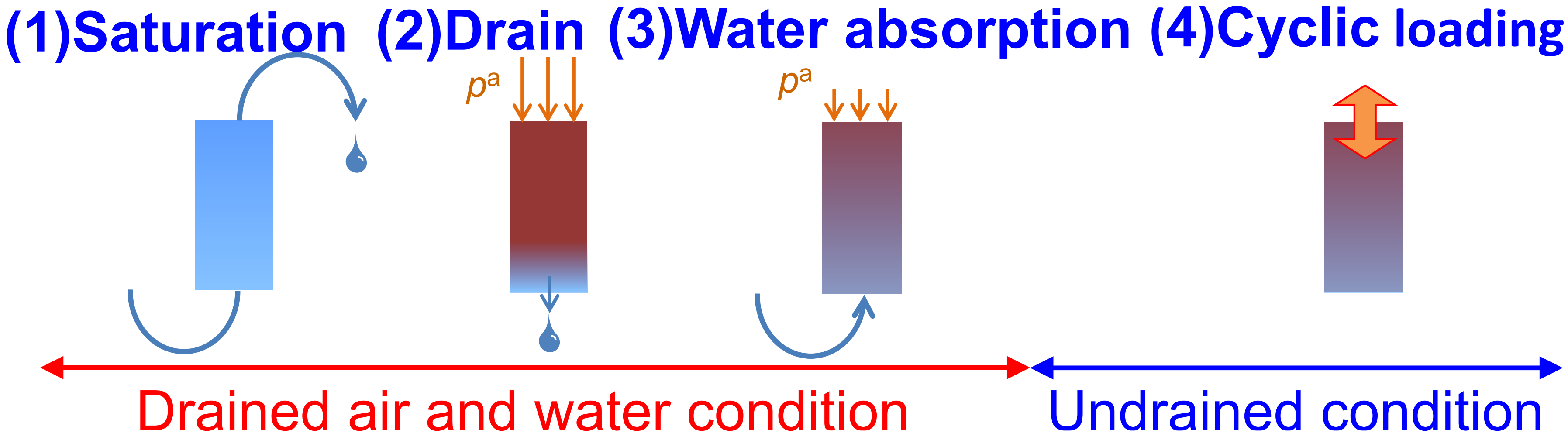

Input axial strain

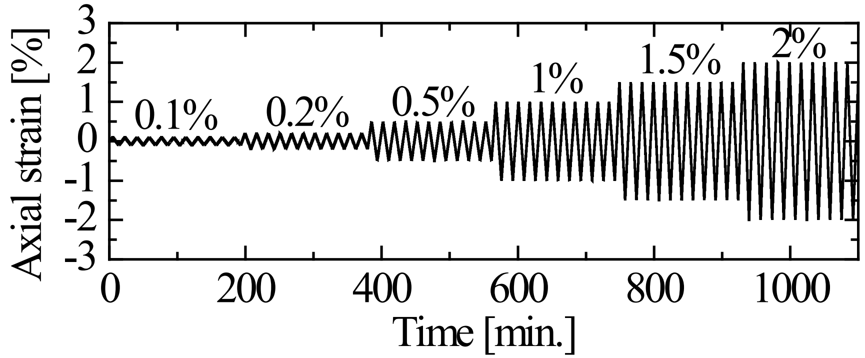

Test cases

Case1： p^c=14kPa

Case2： p^c=4kPa

Case3： p^c=0.3kPa

Cyclic triaxial test of embankment material

The parameters of embankment material were determined from the simulations of cyclic triaxial test.

Experiment

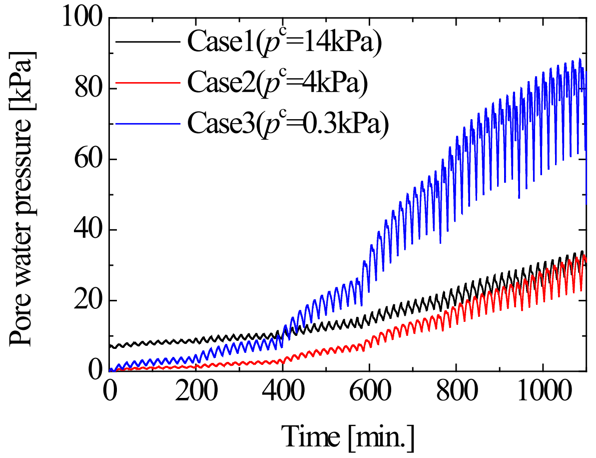

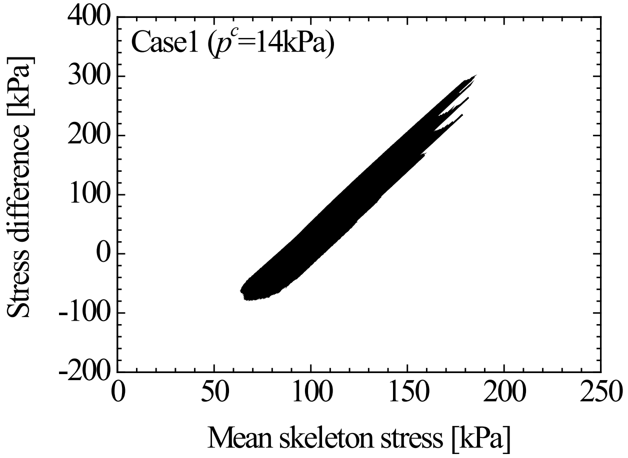

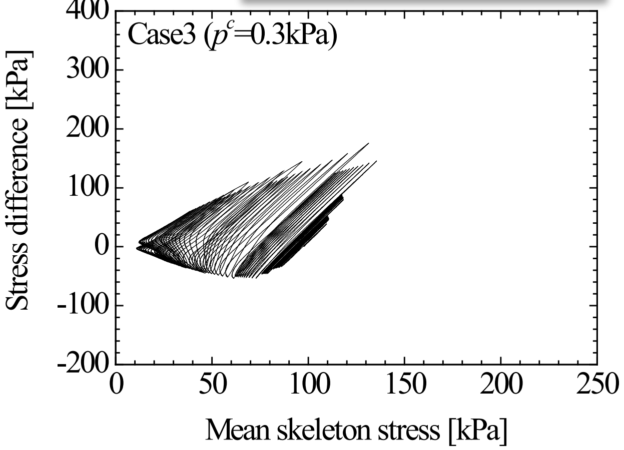

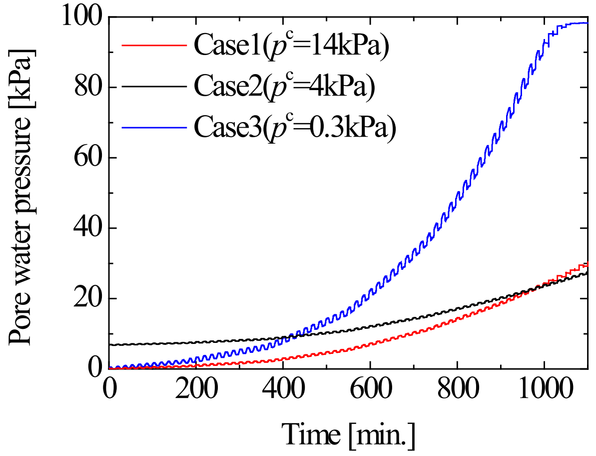

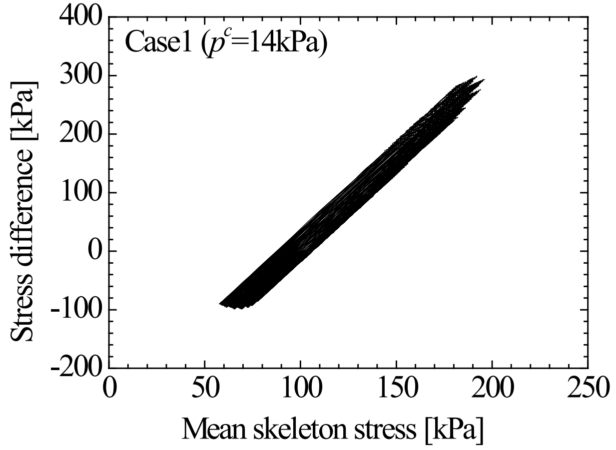

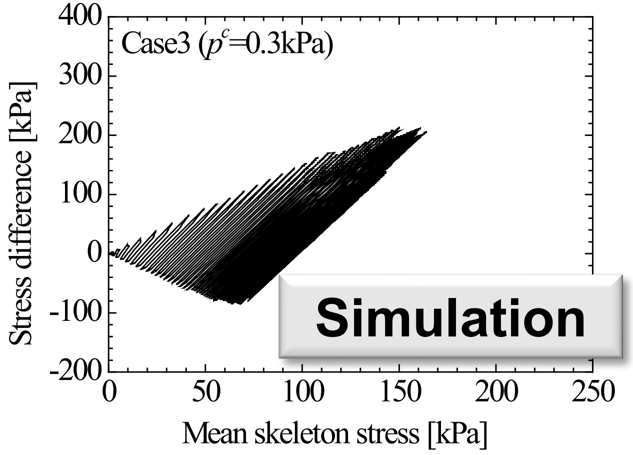

Simulation

The simulations could reproduce the experiments well.

Steps of numerical simulations

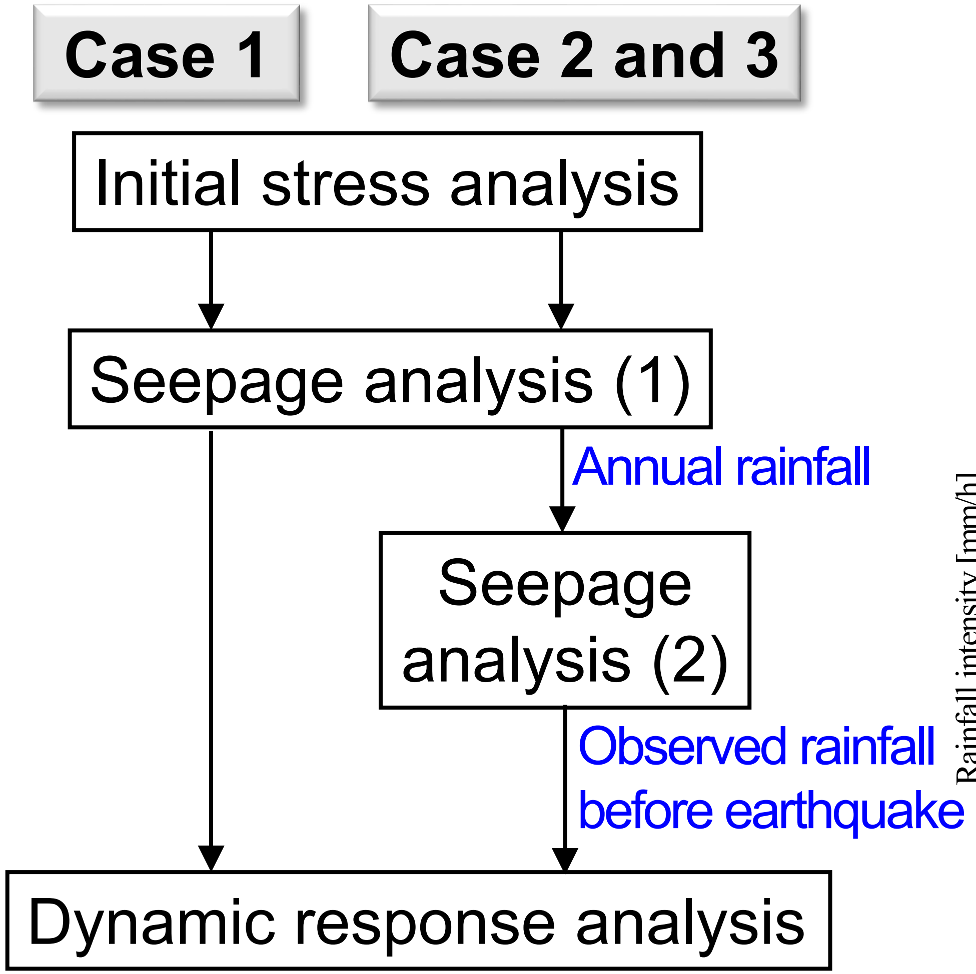

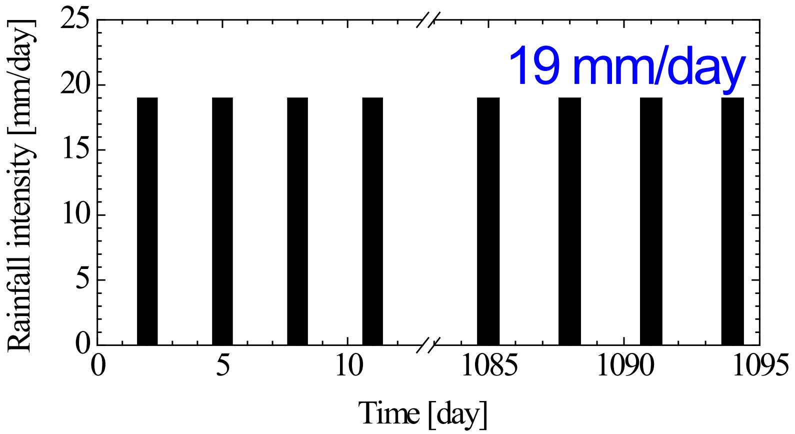

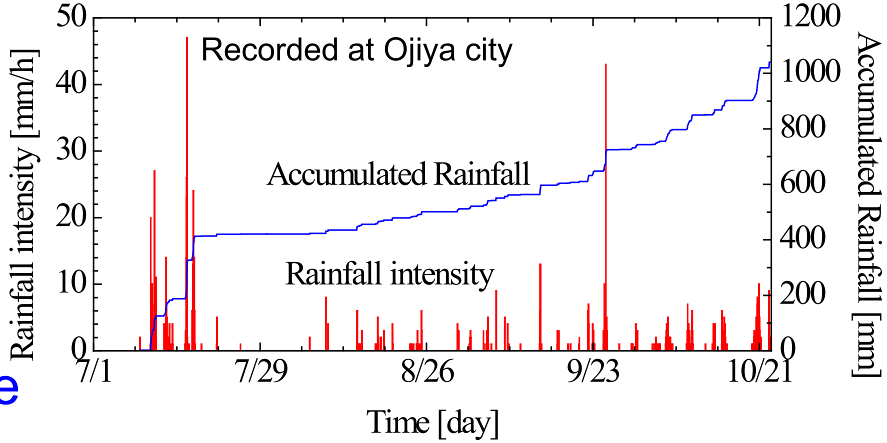

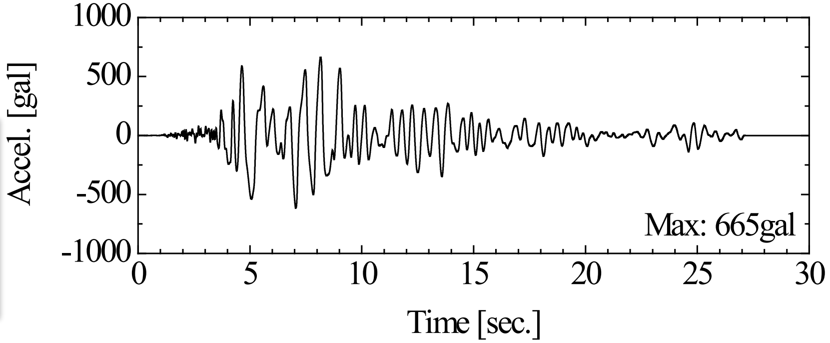

Estimate influence of rainfall to seismic resistance

Analytical conditions

Finite element model

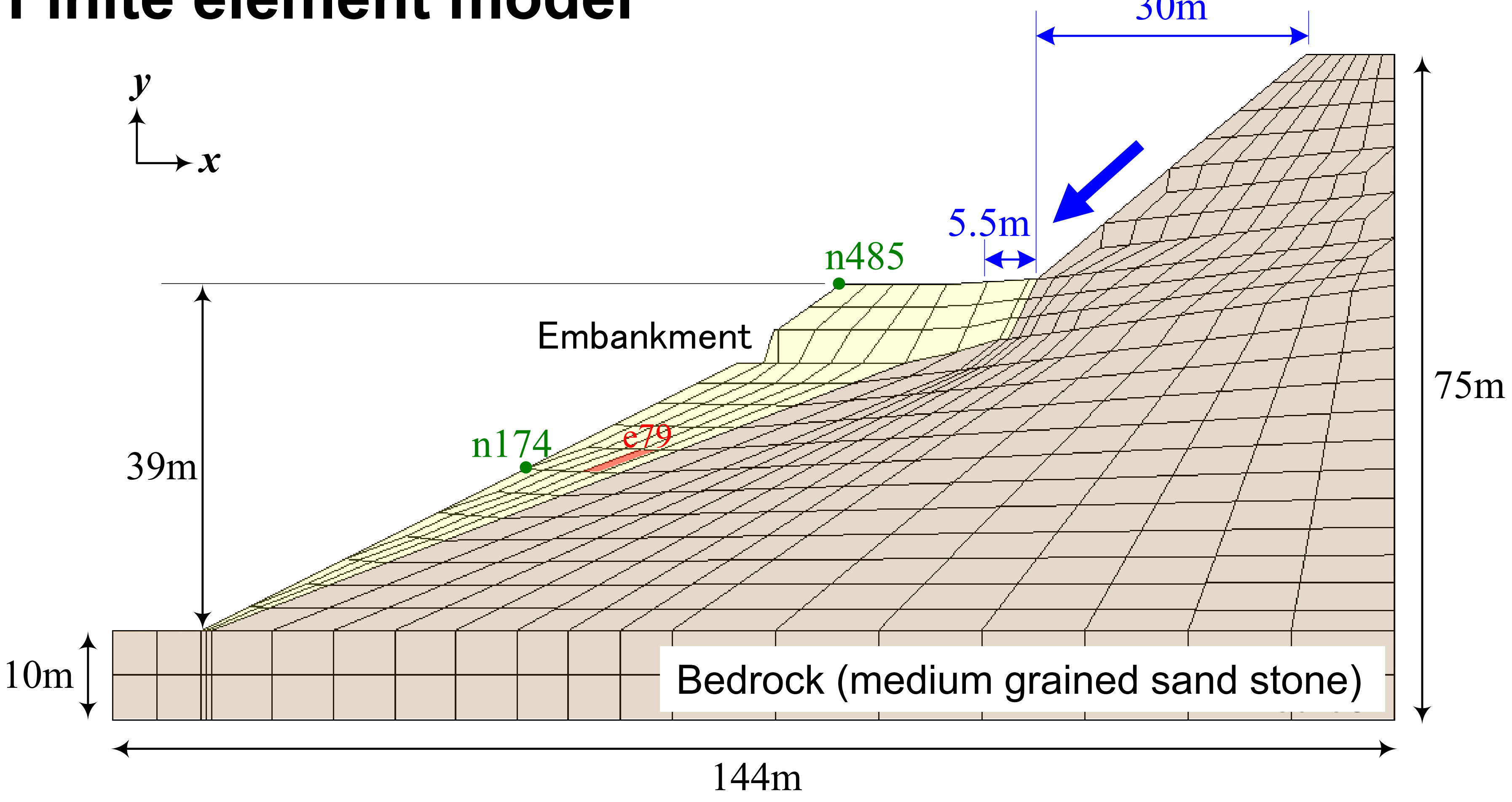

In Case 3, rainfall poured on slope surface above embankment seeped into embankment.

Degree of saturation before earthquake

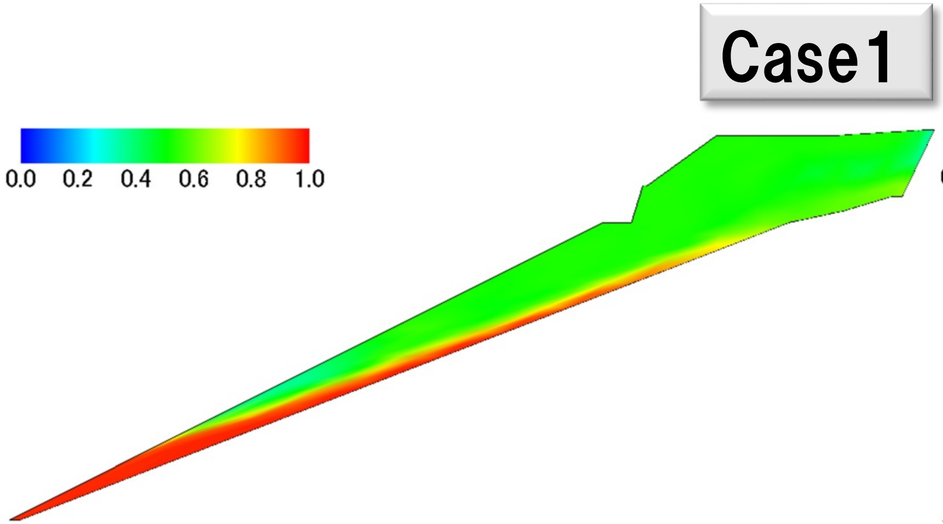

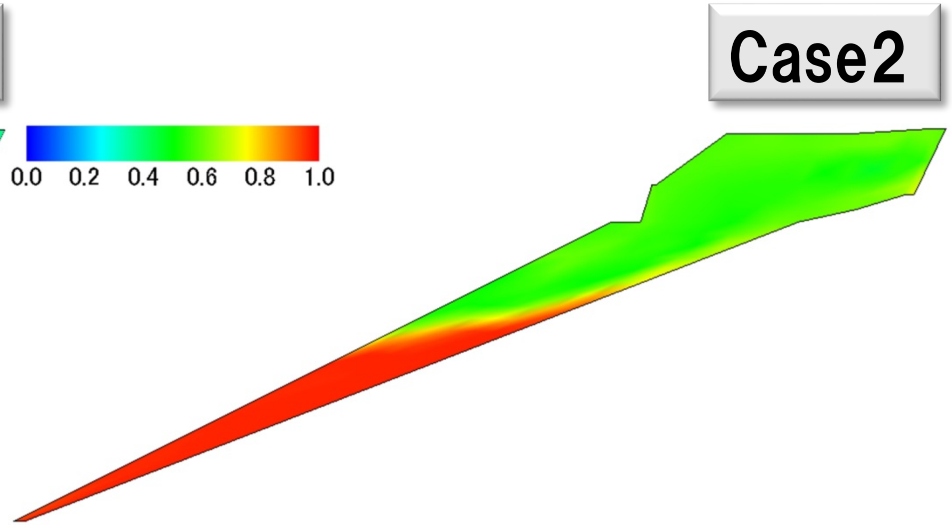

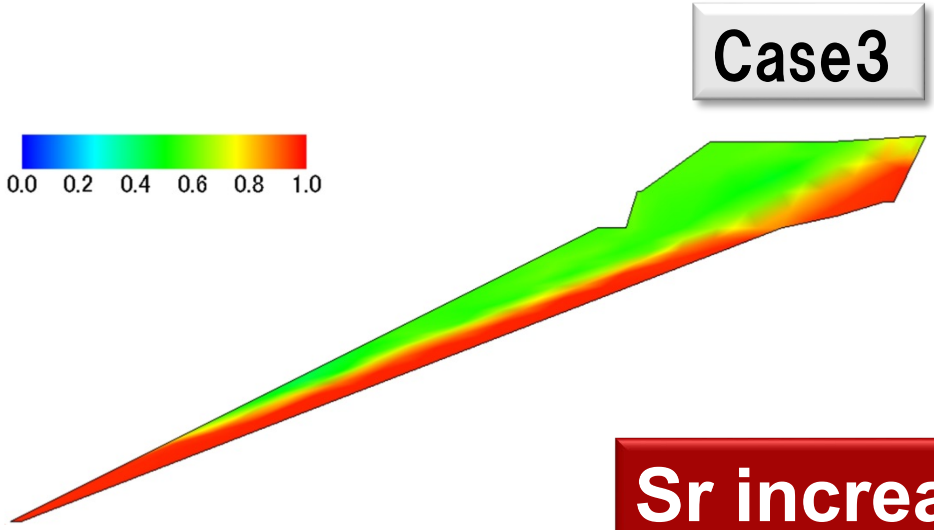

Sr increased more largely at toe in Case 2 and at top in Case 3.

Time histories of vertical displacement

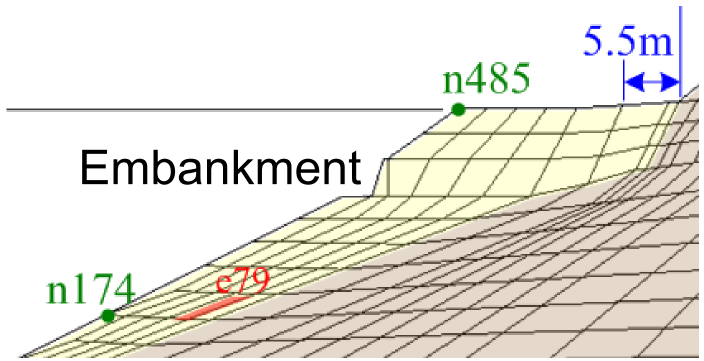

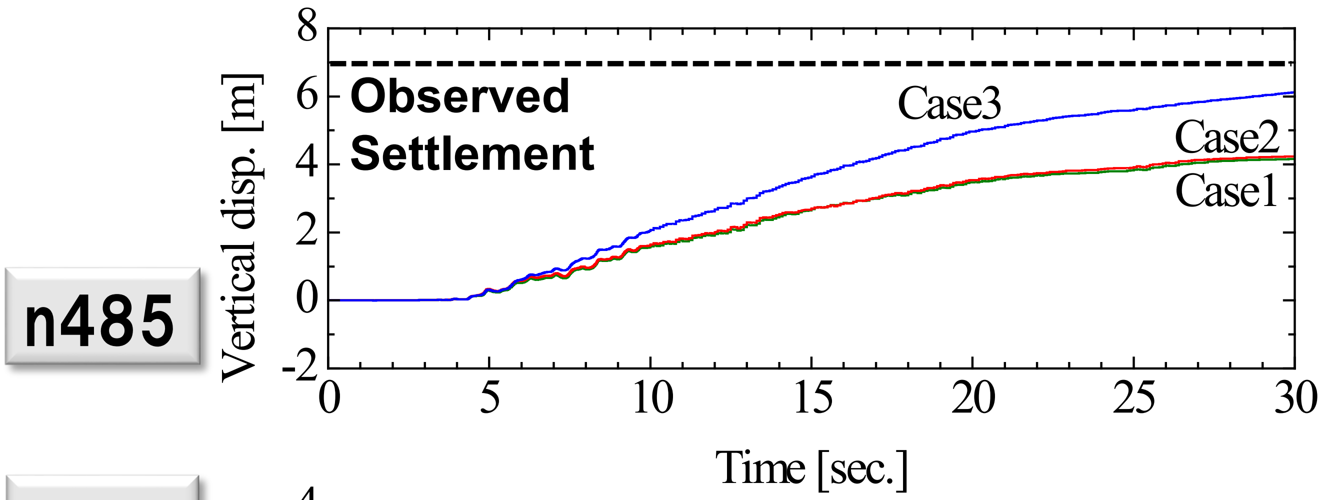

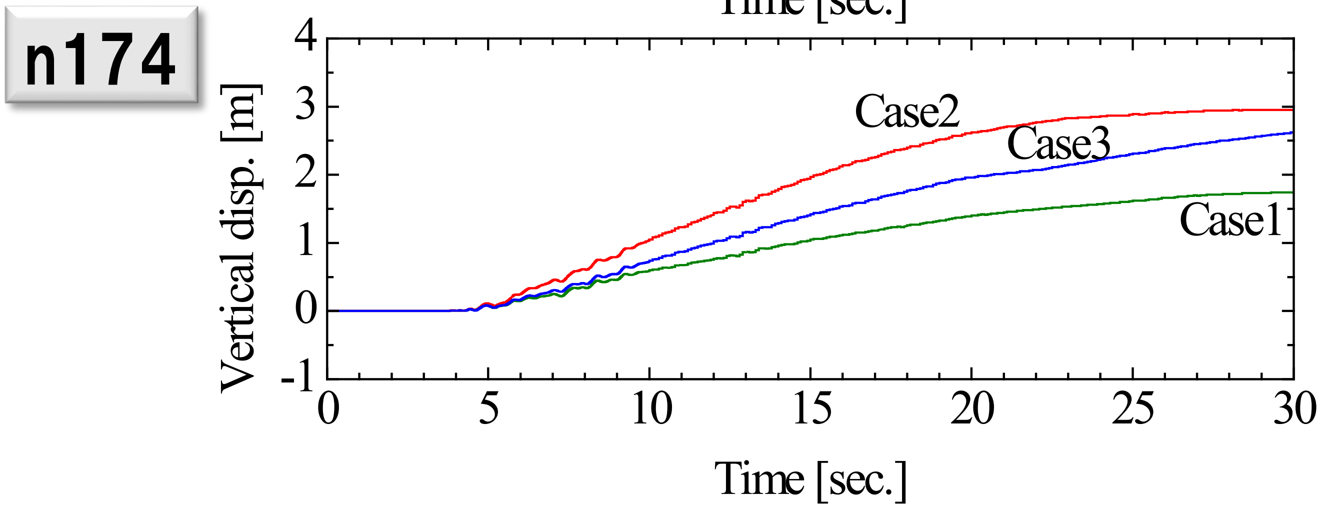

Larger displacement was obtained in Case 2 and 3.

Simulated disp. in Case 3 almost coincided with observed.

Conclusions

Three-phase seepage-deformation coupled analysis focused on damage in the 2004 Niigata-ken Chuetsu earthquake was performed.

By applying the rainfall before the earthquake,

- Degree of saturation increased more widely.
- Dynamic response analysis showed larger deformation and coincidence with measured.
- Liquefaction would occur in embankment and cause large strain.

地盤の動的解析における物理探査（地盤調査）

- 良質な不かく乱試料を用いた室内試験がない場合、原位置試験から力学的材料パラメータを経験的に推定する場合がある。物理探査で力学的材料パラメータを合理的に推定できると有用。
- 地震前の斜面や盛土の初期条件（地下水位、飽和度分布）がその後の地震時挙動に影響するので正確に把握する必要がある。物理探査が時々刻々変化する初期条件をを推定できると有用。
- 地震後の斜面や盛土の変状がその後の降雨浸透挙動に影響する。地震後の斜面や盛土内の状態を物理探査で知ることができると有用。

Xu, J., Ueda, K., & Uzuoka, R. (2021). Evaluation of failure of slopes with shaking-induced cracks in response to rainfall. *Landslides 2021*, 1–18. https://doi.org/10.1007/S10346-021-01734-1

1.3 Objectives and methods

The study of slope response to post-shaking rainfall is lacking but highly demanded.

Objectives

1. To examine slope's performance under different external conditions (rainfall; shaking and rainfall);
2. To evaluate the effect of shaking-induced cracks on the seepage and deformation of slope during the subsequent rainfall;
3. To evaluate the effect of shaking intensity and rainfall intensity on landslide kinematics;
4. To propose a method used for FEM modeling of slope response to post-shaking rainfall.

Methods

1. Centrifuge modeling
2. Numerical simulation

Today only centrifuge modelling is presented here.

2 Centrifuge model tests

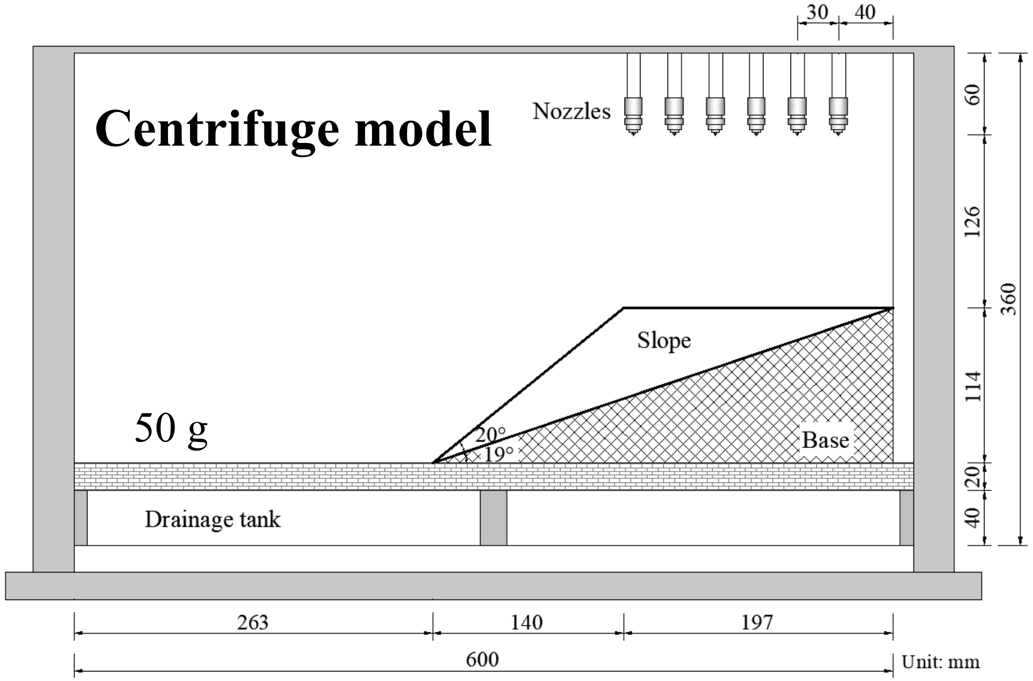

Program

Test	Condition	Shaking intensity	Rainfall intensity
A1	Only rainfall	None	30 mm/h
A2	Shaking and rainfall	4.6 m/s^2	30 mm/h
A3	Repeatability of test A2	4.6 m/s^2	30 mm/h
B1	Only rainfall	None	9 mm/h
B2	Shaking and rainfall	4.6 m/s^2	9 mm/h
B3	Repeatability of test B2	4.6 m/s^2	9 mm/h
C1	Rainfall, shaking, and rainfall	4.6 m/s^2	9 mm/h
C2	Rainfall, shaking, and rainfall	3.0 m/s^2	9 mm/h

Soil information

Property	Value	Property	Value
Dry density	1.50 g/cm^3	Saturation	0.35
Relative density	85 %	Permeability	4.4 mm/h (1.2E-6 m/s)
Void ratio	0.75		

2 Centrifuge model tests

Rainfall simulator

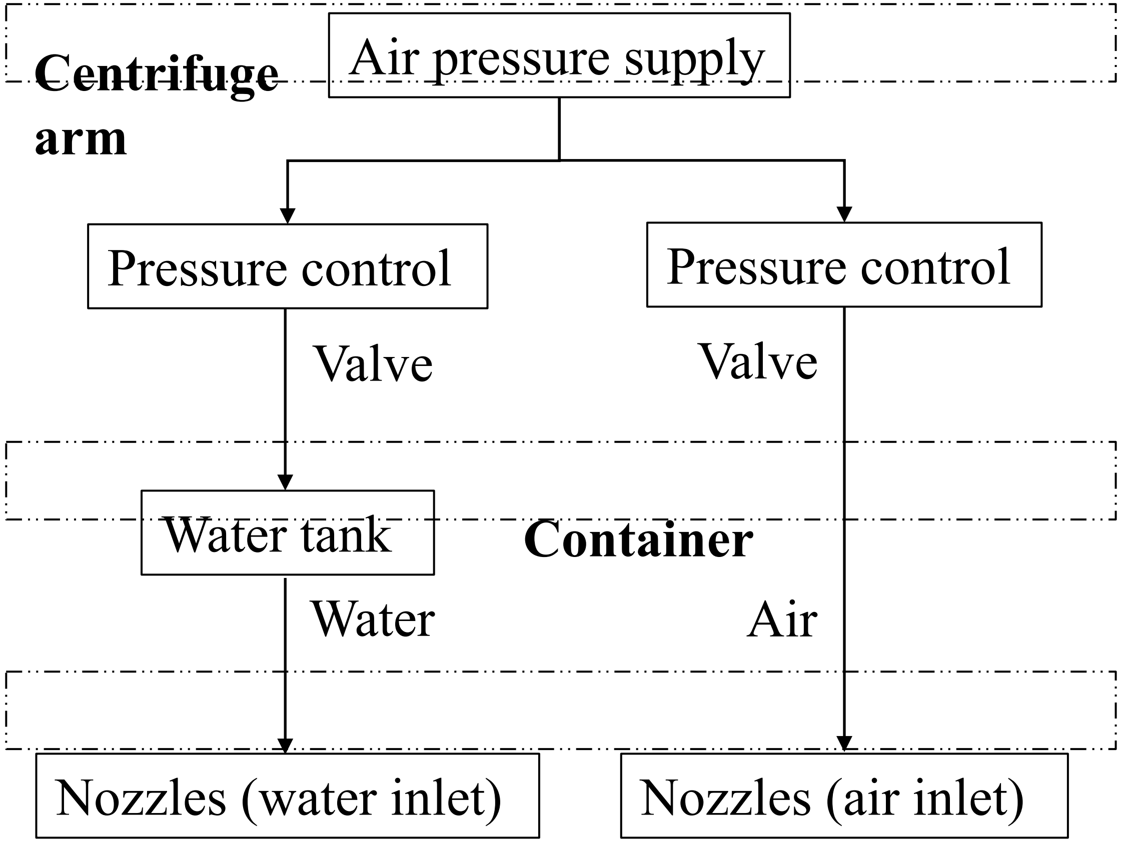

Calibration was conducted to achieve uniform rainfall

Top view of container

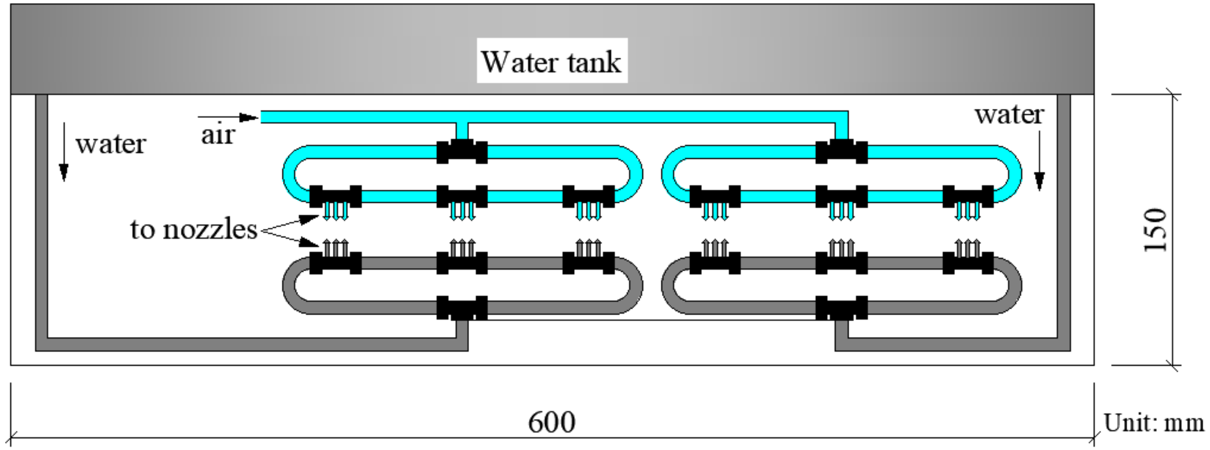

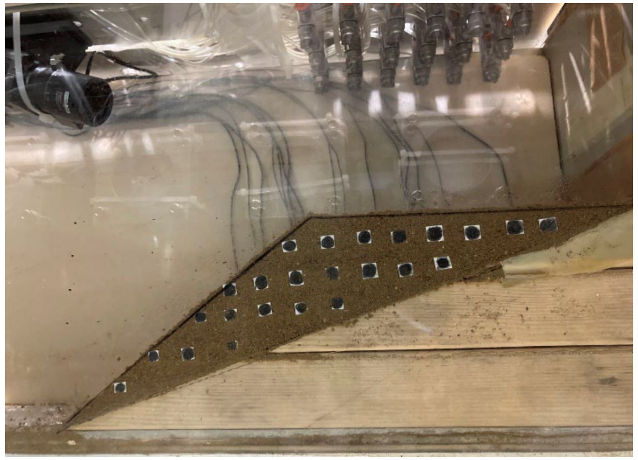

Slope model inside container

2.2 Response of slopes to shaking

Test	Shaking intensity	Rainfall intensity	Condition
A2	4.6 m/s^2	30 mm/h	Shaking and rainfall
B2	4.6 m/s^2	9 mm/h	Shaking and rainfall

Sinusoidal input wave (1 Hz, 40 s)

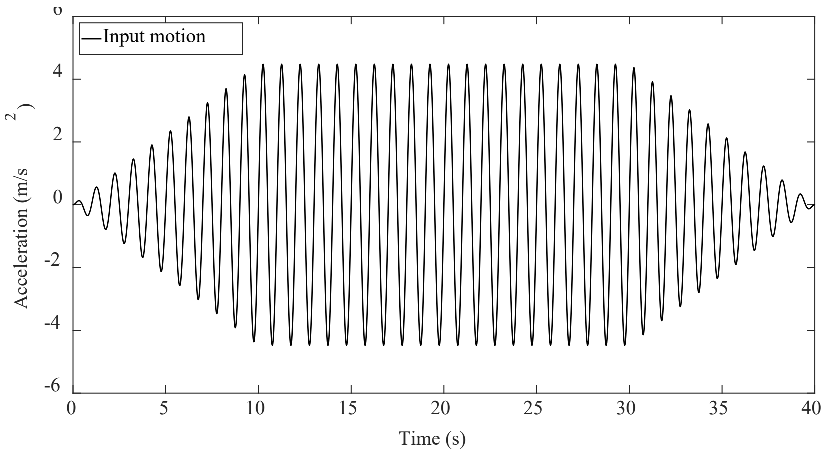

- Displacement vectors

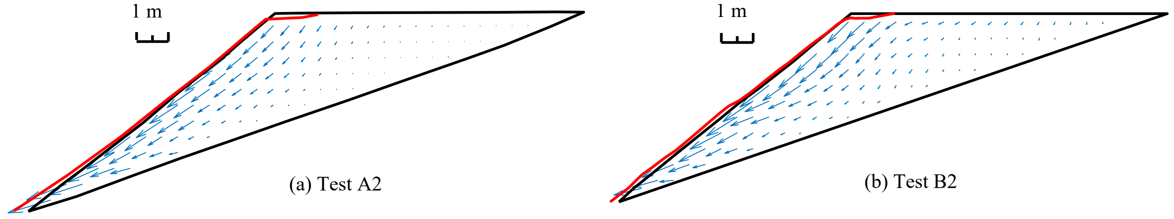

- Top view of slope crest

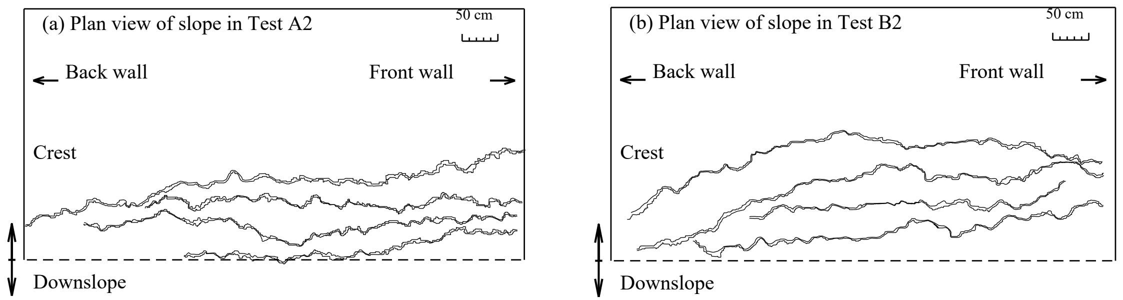

➢ Displacement discontinuity caused cracks near slope shoulder

2.3 Response of slopes to rainfall

Test	Shaking intensity	**Rainfall intensity**	Condition
A1	None	30 mm/h	Rainfall
A2	4.6 m/s^2	30 mm/h	Shaking and rainfall
B1	None	9 mm/h	Rainfall
B2	4.6 m/s^2	9 mm/h	Shaking and rainfall

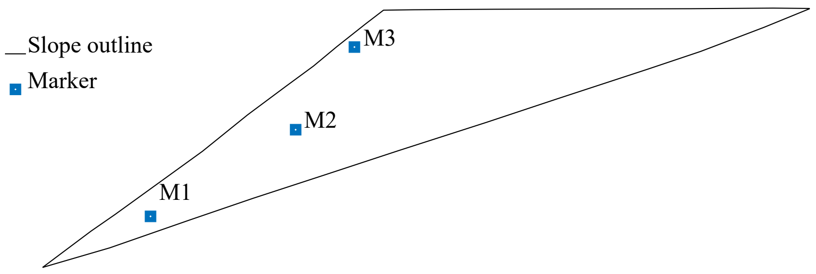

- Soil displacement during rainfall

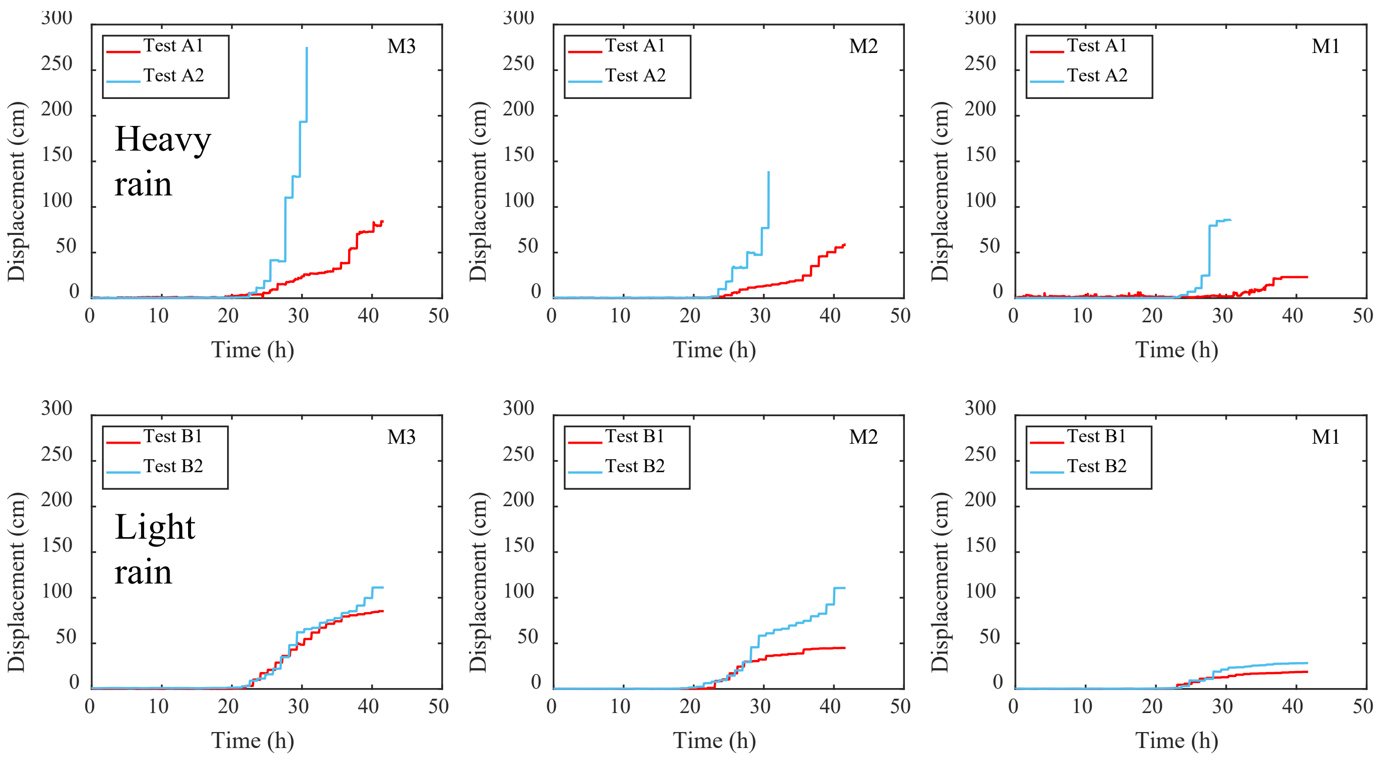

➢ Heavy rainfall accelerated the failure of slope with cracks

2.3 Response of slopes to rainfall

- Slope deformation

(a) Test A1, heavy rain

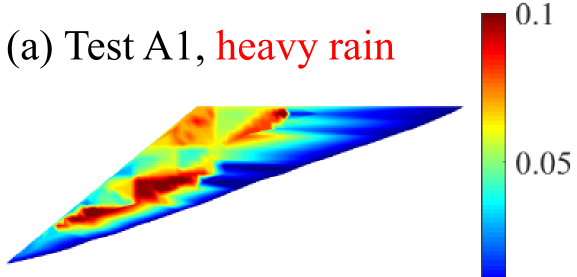

(a) Incremental equivalent strain at the onset of rainfall-induced landslide in test A1

(c) Test A2, post-shaking heavy rain

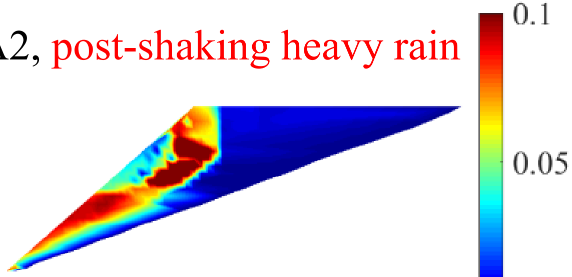

(c) Incremental equivalent strain at the onset of rainfall-induced landslide in test A2

(b) Test B1, light rain

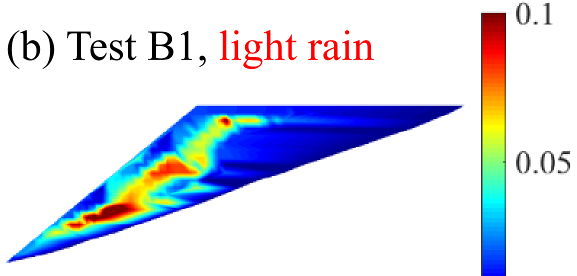

(b) Incremental equivalent strain at the onset of rainfall-induced landslide in test B1

(d) Test B2, post-shaking light rain

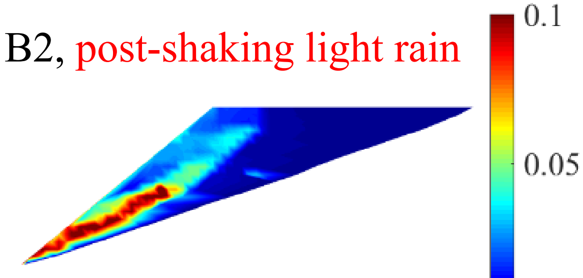

(d) Incremental equivalent strain at the onset of rainfall-induced landslide in test B2

- Slope after failure

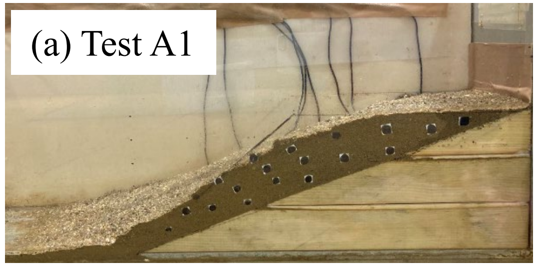

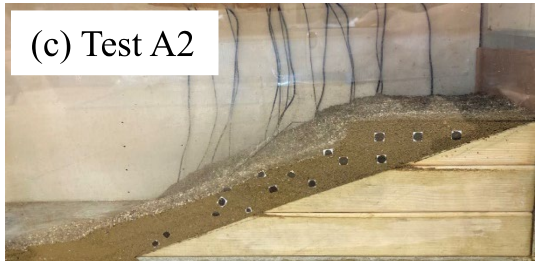

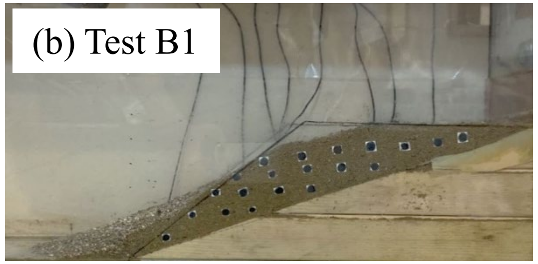

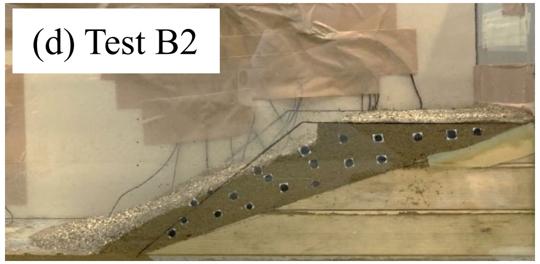

- ➢ Shaking-induced cracks changed landslide features during rainfall
- ➢ Rainfall intensity controlled landslide features of slopes with cracks

2.3 Response of slopes to rainfall

Test	Shaking intensity	Rainfall intensity	Condition
A1	None	30 mm/h	Rainfall
A2	4.6 m/s^2	30 mm/h	Shaking and rainfall
B1	None	9 mm/h	Rainfall
B2	4.6 m/s^2	9 mm/h	Shaking and rainfall

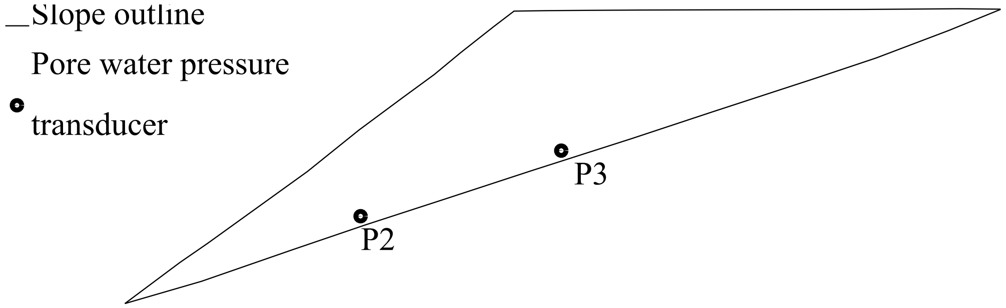

- Effect of rainfall intensity on preferential flow

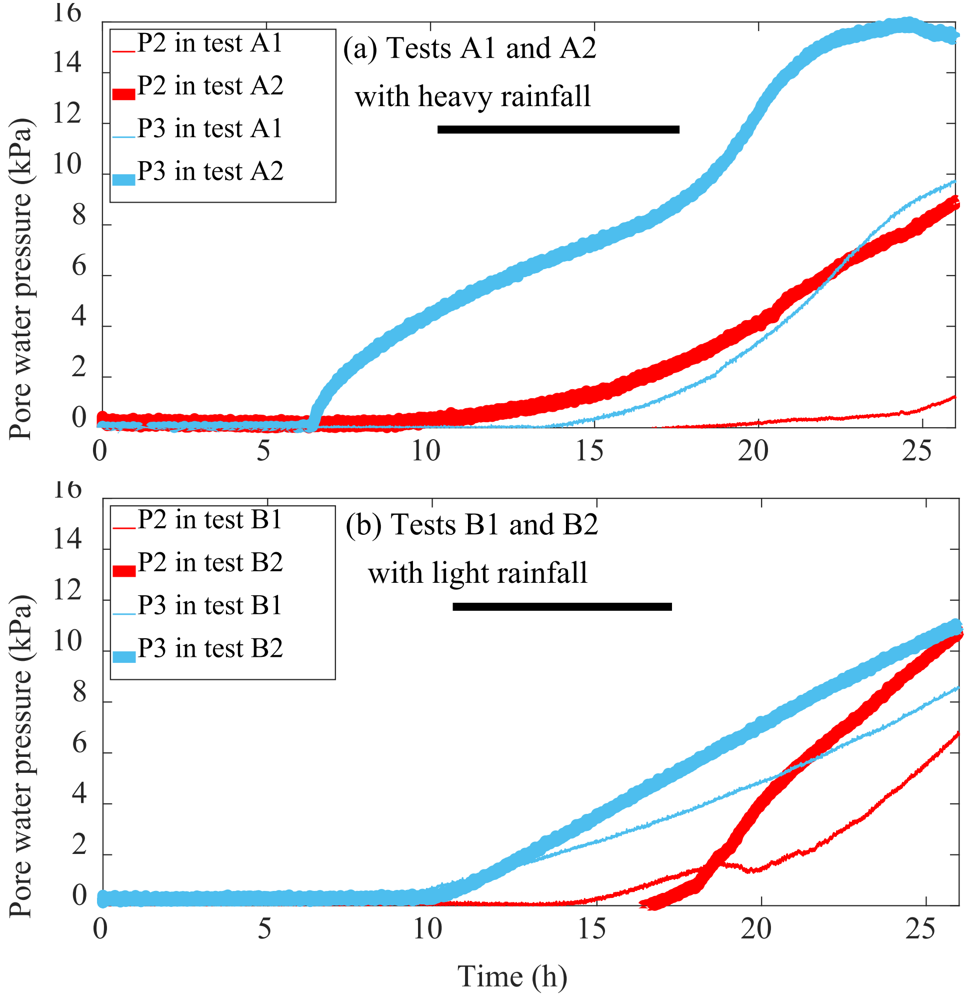

➢ Preferential flow due to cracks was evident during heavy rainfall

4 Conclusions

Experiments

1. Once shaking caused cracks on the slope surface, the pattern and severity of the slope failure caused by the following rainfall became different, compared with the slope subject to only rainfall.

2. Shaking-induced cracks changed landslide features during rainfall and heavy rainfall accelerated the failure of slope with cracks.

3. The effect of cracks on preferential flow depended on the rainfall intensity.

地盤の動的解析における物理探査(地盤調査)

- 良質な不かく乱試料を用いた室内試験がない場合、原位置試験から力学的材料パラメータを経験的に推定する場合がある。物理探査で力学的材料パラメータを合理的に推定できると有用。
- 地震前の斜面や盛土の初期条件(地下水位、飽和度分布)がその後の地震時挙動に影響するので正確に把握する必要がある。物理探査が時々刻々変化する初期条件をを推定できると有用。
- 地震後の斜面や盛土の変状がその後の降雨浸透挙動に影響する。地震後の斜面や盛土内の状態を物理探査で知ることができると有用。

Recent geophysical survey

Integrated geophysical investigation of river levee

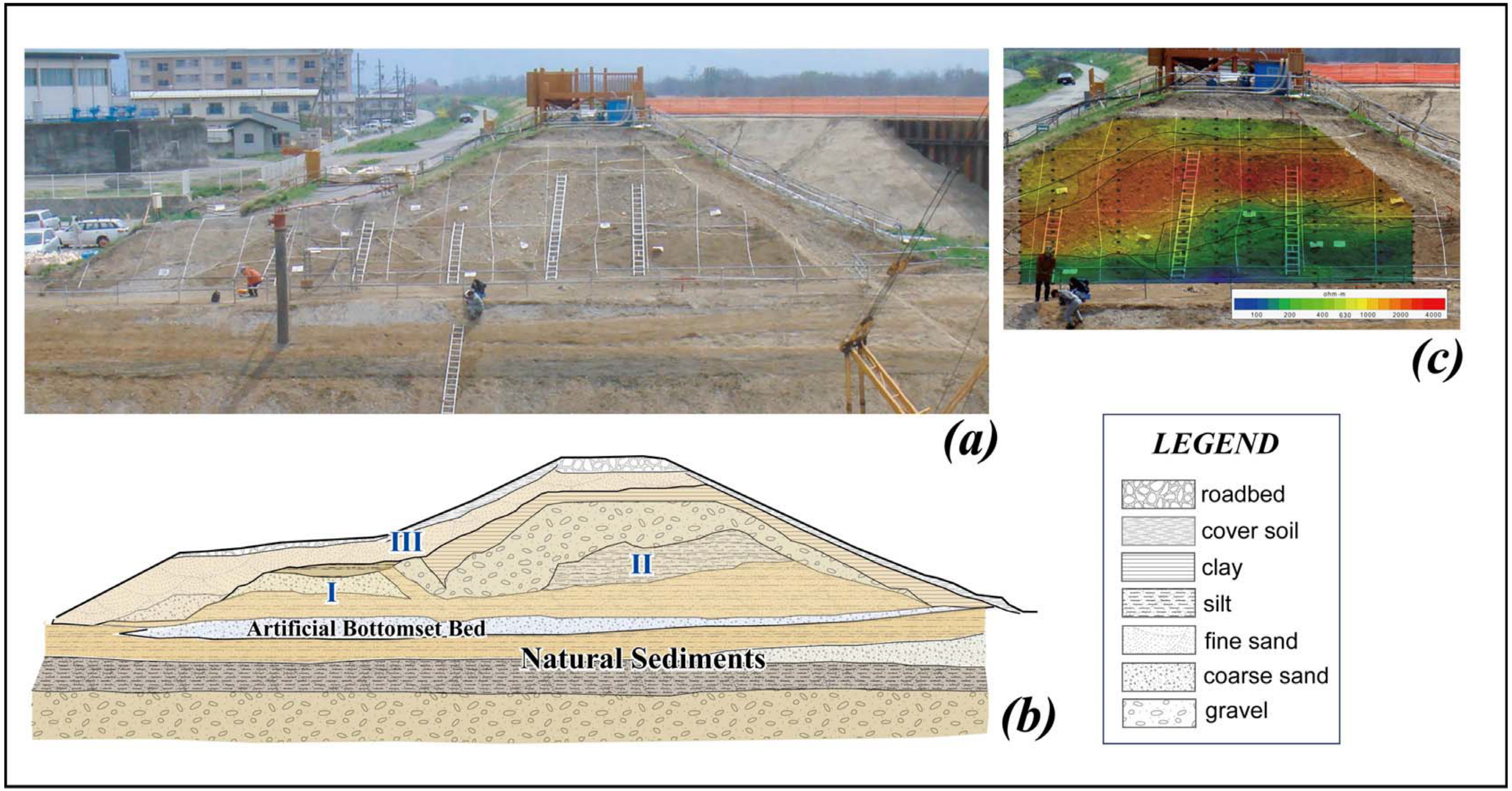

Figure 5. Field observations and measurement results at an open-cut. ***(a)***: Photograph of the excavated outcrop. The internal structure of the levee body is visible. The layered structure of the underlying natural sediments is also recognizable. ***(b)***: Geological sketch of the open-cut slope. Three construction stages are interpreted from the stacking structure of the materials. ***(c)***: Resistivity map of the open-cut surface reconstructed using 125 data points.

(Inazaki et al. 2008)

Integrated geophysical investigation of river levee

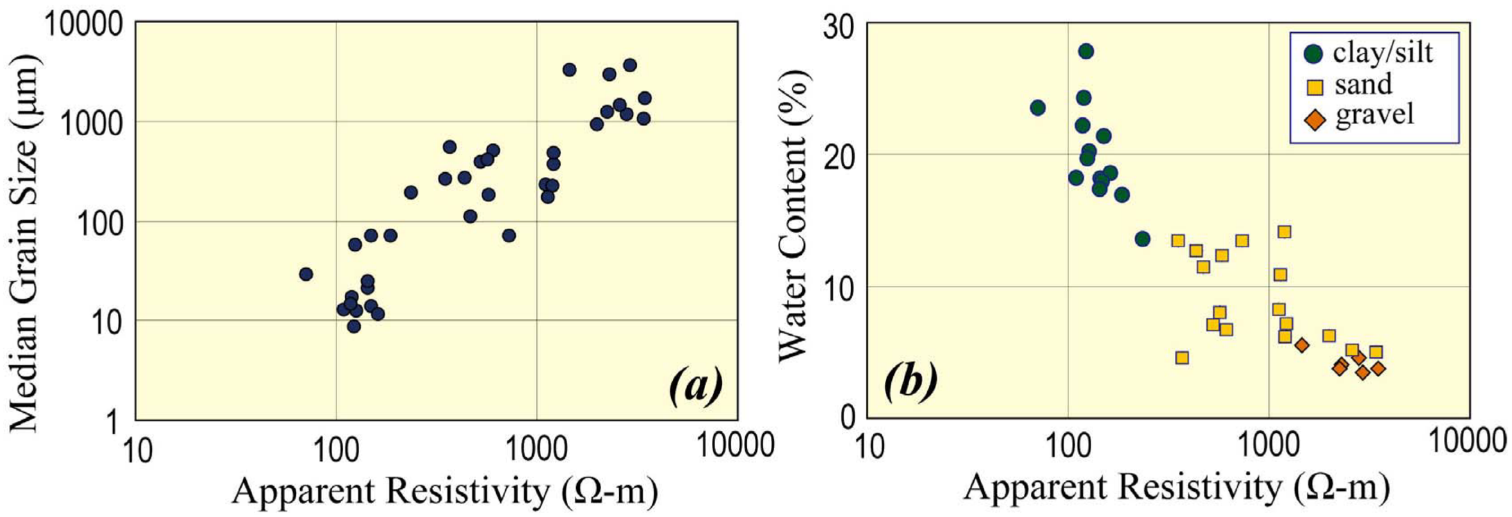

Figure 6. Relationship between resistivity and grain size ***(a)*** and water content ***(b)***. There is a direct relationship between apparent resistivity and median grain size (both in log scale). In contrast, the water content shows a negative relationship with apparent resistivity.

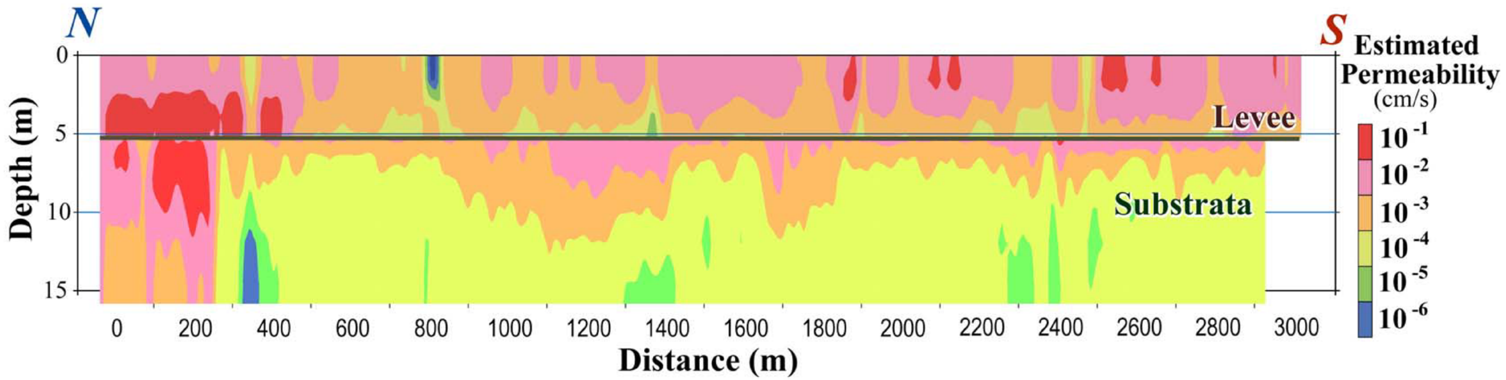

Figure 8. A permeability profile model along the Chikuma 56R line estimated from resistivity data. High permeable zones were interpreted in the levee body as well as in the underlying sediments. Locations of the interpreted high permeability zones were basically concordant with those where seepage had occurred.

(Inazaki et al. 2008)

Soil permeability profiling using geophysical data

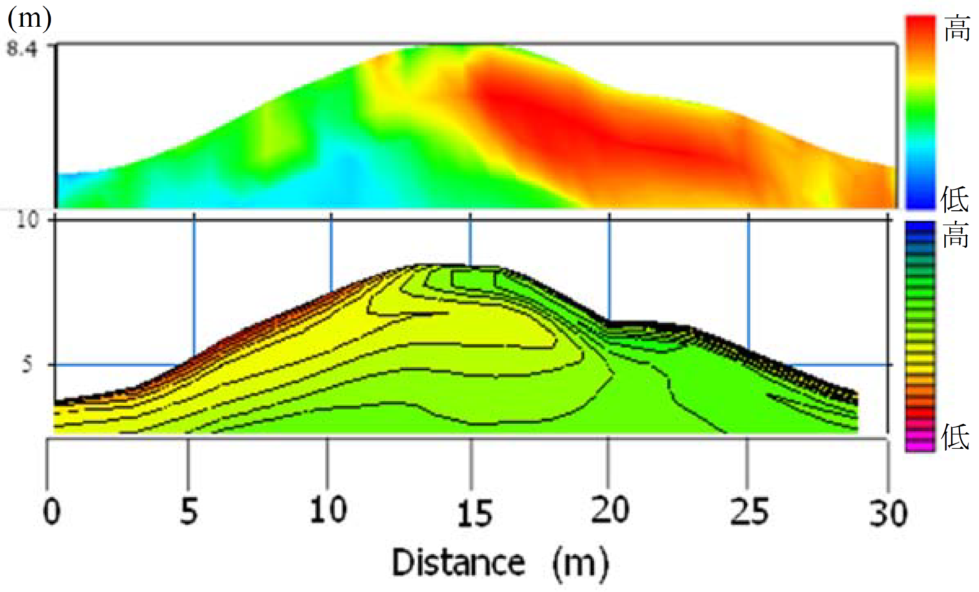

図 2　探査で得られた比抵抗(上)と S 波速度断面(下)
Fig.2 Resistivity(upper) and S-wave velocity profiles(bottom)

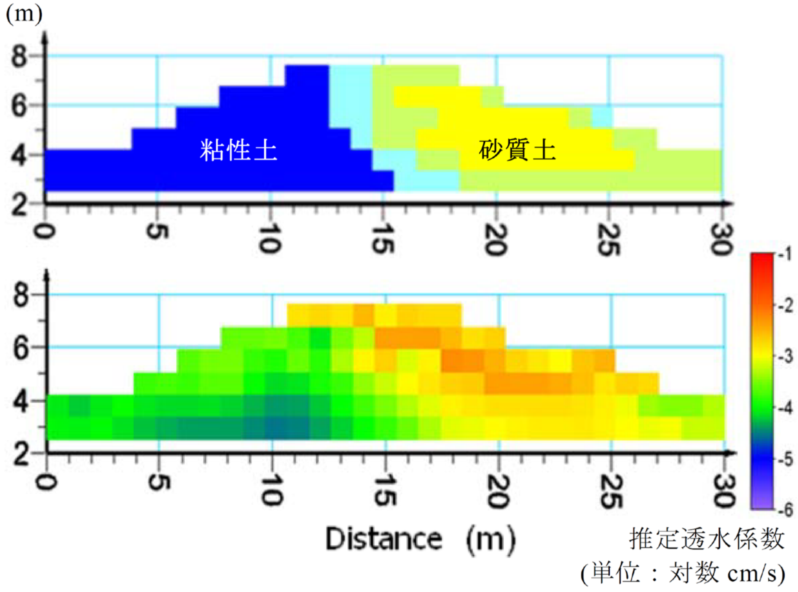

図 3　探査データから推定した土質(上)及び透水係数断面(下)
Fig.3 Estimated Soil (upper) and permeability profiles(bottom)

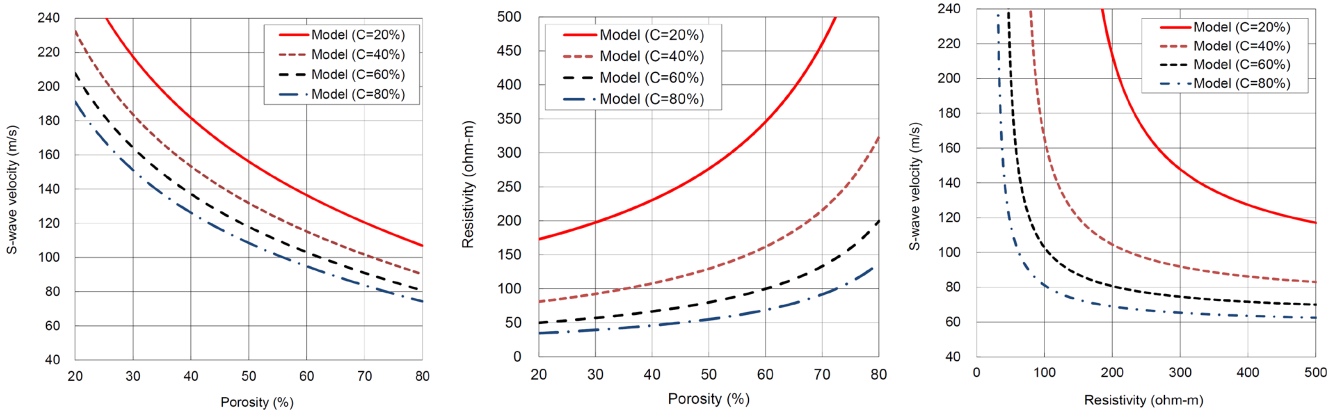

図-1 S 波速度と間隙率（左），比抵抗と間隙率（中），S 波速度と比抵抗（右）の計算結果（C：粘土含有率）
Fig. 1 Calculated relationships of S-wave velocity-porosity (left), resistivity-porosity (middle) and S-wave velocity – resistivity(right). C is the clay content.

(Takahashi et al. 2018)

Modelling time-lapse shear-wave velocity changes

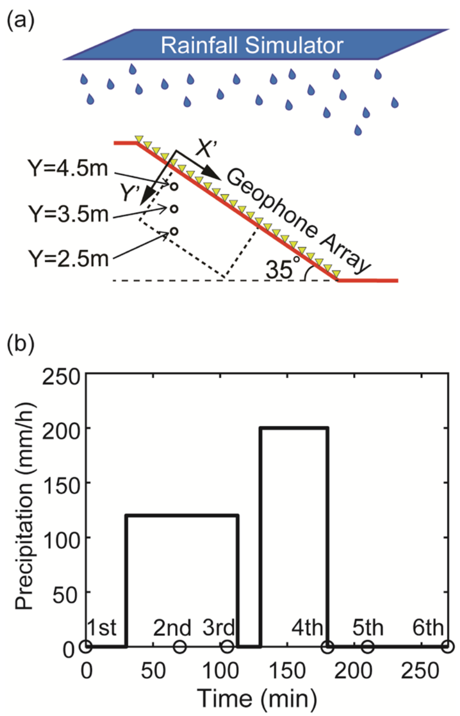

Figure 6: (a) Cross-section of the field-scale test embankment and the location of the fixed geophone array. Small open circle are the locations where the temporal changes are monitored (from time-lapse surface wave dispersion data) and shown in Figure 8(a). Dashed rectangle shows the spatial range of the V_s distribution shown in Figure 8(b). (b) The time series of rainfall in this field-scale measurement. Seismic surface wave measurements are made at the time shown by open circles in (b).

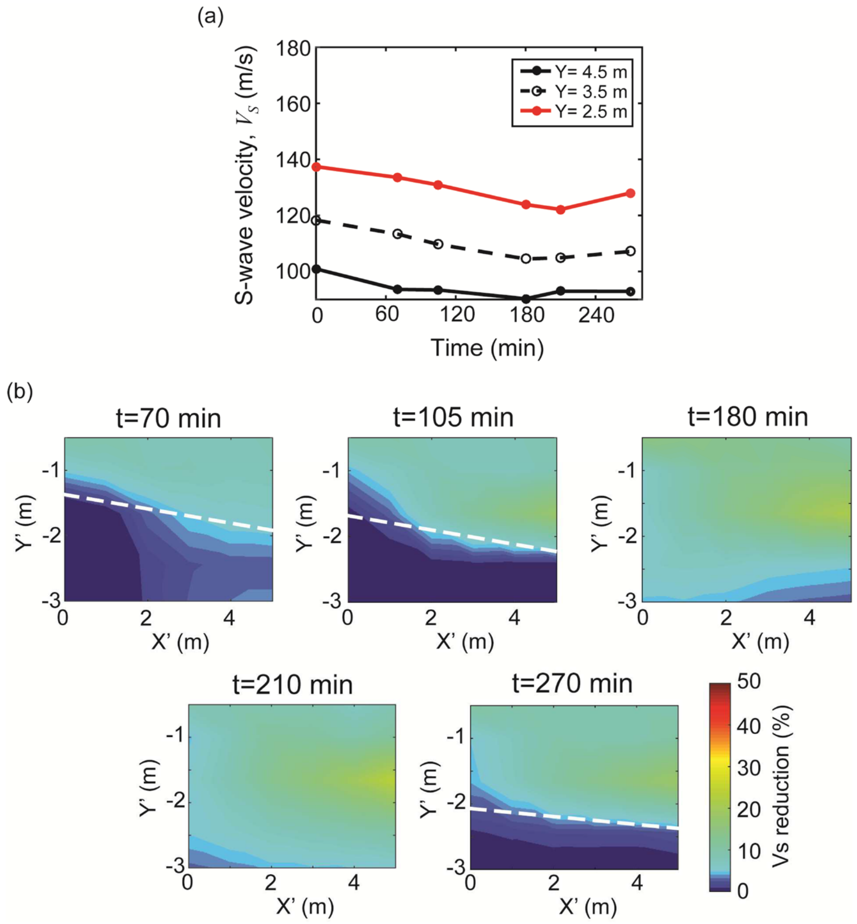

Figure 8: (a) Observed temporal changes of V_S in the field-scale experiment (modified after Konishi et al., 2015). Values at three spatial locations (small open circles in Figure 6(a)) are shown. (b) Spatial distribution of the V_S reduction rate R (equation 7) at each measurement (modified after Konishi et al., 2015). Positive values of R indicate a decrease of V_S from the initial values. White dashed lines mark the position of the boundary representing sharp changes in the V_S reduction rate, which is interpreted as to be indicating water infiltration and drainage.

$$R(\%) = \frac{V_S(t=0) - V_S(t)}{V_S(t=0)} \times 100.$$

(Suzaki et al. 2017)

地盤の動的解析における物理探査（地盤調査）

- 良質な不かく乱試料を用いた室内試験がない場合、原位置試験から力学的材料パラメータを経験的に推定する場合がある。物理探査で力学的材料パラメータを合理的に推定できると有用。
- 地震前の斜面や盛土の初期条件（地下水位、飽和度分布）がその後の地震時挙動に影響するので正確に把握する必要がある。物理探査が時々刻々変化する初期条件をを推定できると有用。
- 地震後の斜面や盛土の変状がその後の降雨浸透挙動に影響する。地震後の斜面や盛土内の状態を物理探査で知ることができると有用。